

# Kinematic evolution of the eastern Tethyan Himalaya: constraints from magnetic fabric and structural properties of the Triassic flysch in SE Tibet

BORJA ANTOLÍN<sup>1\*</sup>, ERWIN APPEL<sup>1</sup>, CHIARA MONTOMOLI<sup>2</sup>, ISTVÁN DUNKL<sup>3</sup>, LIN DING<sup>4</sup>, RICHARD GLOAGUEN<sup>5</sup> & RACHIDA EL BAY<sup>1</sup>

<sup>1</sup>*Institute for Geosciences, University of Tuebingen, Sigwartstrasse 10, 72076 Tuebingen, Germany*

<sup>2</sup>*Department of Earth Sciences, University of Pisa, via S. Maria 53, 56126 Pisa, Italy*

<sup>3</sup>*Institute for Geosciences, University of Göttingen, Goldschmidtstrasse 3, D-37077 Göttingen, Germany*

<sup>4</sup>*Institute of Tibetan Plateau Research, Chinese Academy of Sciences, Shuangqing Rd. 18, Beijing 100085, China*

<sup>5</sup>*Department of Geology, Technical University of Freiberg, Bernhard-von-Cottastrasse 2, 09596 Freiberg, Germany*

*\*Corresponding author (e-mail: borjapinzas@hotmail.com)*

**Abstract:** Anisotropy of magnetic susceptibility (AMS) combined with structural analysis are used in this work with the aim to characterize the tectonic evolution of the Triassic flysch within the eastern Tethyan Himalaya Thrust Belt in SE Tibet. The attitude of the magnetic foliation and lineation are concordant with the planar and linear structures of tectonic origin defined by the preferred orientation of the iron-bearing silicates. Two different tectonic domains can be defined: (a) the southern domain is controlled by the Eohimalayan tectonic foliation (S1) recorded in the magnetic foliation which trends east–west and dips to the north; (b) the northern domain is dominated by the Neohimalayan magnetic foliation with WNW–ESE strike and dips to the south opposite to the vergence of the main structures. A slightly prolate magnetic ellipsoid has been found in between the two domains recording the intersection of S1 and the subtle development of the S2 tectonic foliation. Hinterland propagation of the deformation lead to the Great Counter backthrust generation, pointed out by the SSW steeply plunging magnetic lineation. Furthermore different orientations of magnetic foliation may indicate an Early Miocene *c.* 20° clockwise vertical-axis rotation.

The collision of India into Eurasia resulted in large-scale shortening of ‘Greater India’ and the consequent development of the Himalayan chain in the Early Tertiary (*c.* 55–50 Ma) (e.g. Searle 1986; Gaetani & Garzanti 1991; Patzelt *et al.* 1996; Najman *et al.* 2005). The Tibetan Plateau and its bordering orogenic mountain belts like the Himalaya provide one of the best natural laboratories to study continental collision processes. The Himalayan orogen has a length of *c.* 2500 km between the Nanga Parbat and the Namche Barwa peaks. These extreme points are geologically called Western and Eastern Syntaxis respectively (Fig. 1a, b).

The present study is focused in a key area of the eastern Himalayan belt in SE Tibet, close to the

Eastern syntaxis, where the structural style changes from frontal collision along the Himalaya to dextral shear between Indian and Asian plates as indicated by GPS observations and Quaternary fault slip rates (Holt *et al.* 1991). Furthermore the study area belongs to the Tethyan Himalaya which represents the carapace to mid-crustal rocks whose exhumation mechanism is under discussion (e.g. Godin *et al.* 2006; Kellett & Godin 2009). To better understand the processes we focus our study in the Triassic flysch of the Tethyan Himalaya in order to obtain better constraints on the kinematic evolution and structural style of folds and thrusts since the India–Asia collision. In the remote area of SE Tibet a very long (*c.* 80 km) and continuous section of Triassic flysch of Tethyan Himalaya

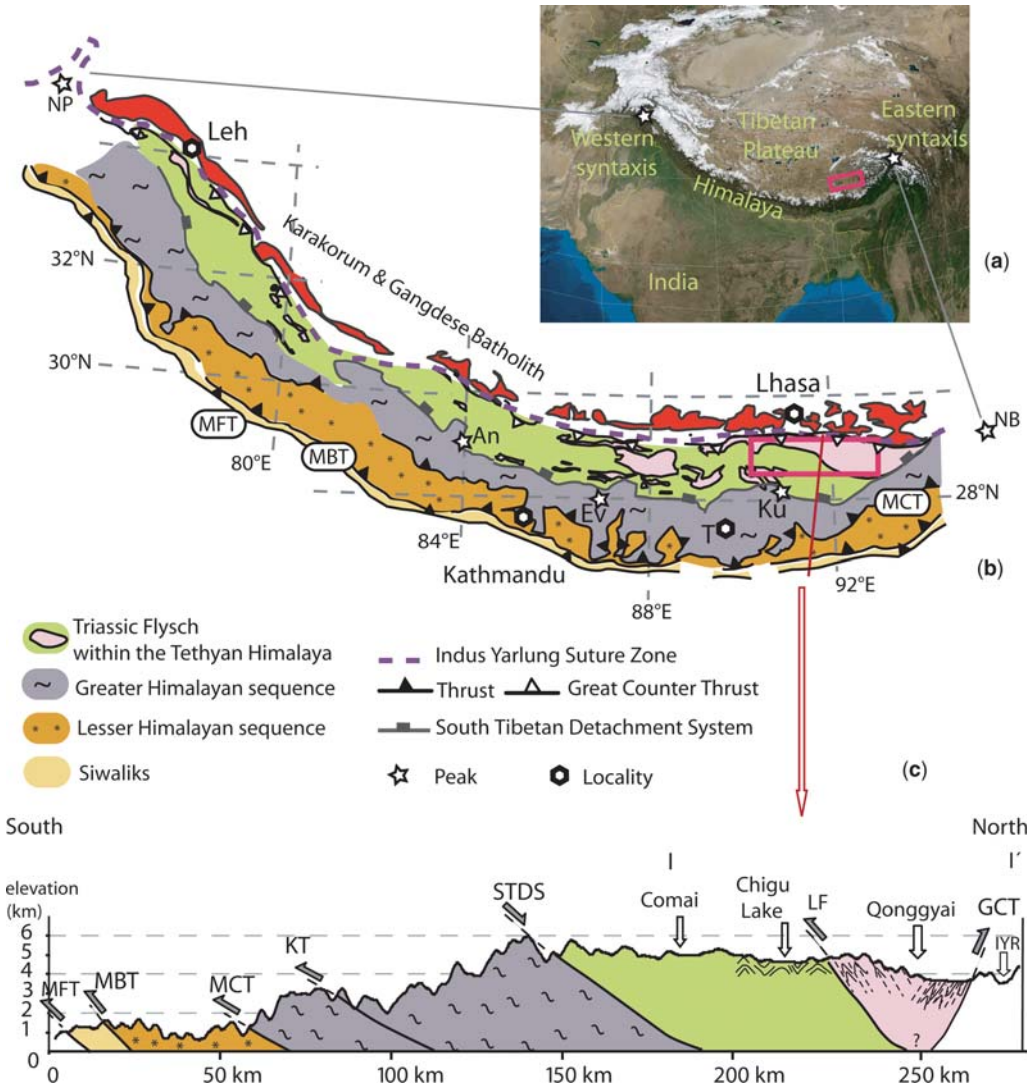


**Fig. 1.** (a) Satellite image of the Himalayan-Tibetan orogen and surrounding area. (b) Geological sketch map of the Himalayan chain after Steck (2003), Pan *et al.* (2004) and Yin (2006). A rectangle shows the location of the studied area. MFT, Main Frontal Thrust; MBT, Main Boundary Thrust; MCT, Main Central Thrust; NP, Nanga Parbat; An, Annapurna; E, Everest; Ku, Khula Kangri; NB, Namche Barwa; T, Timphu. (c) Simplified cross-section of the eastern Himalayas; location in Figure 1b; topographic profile from DEM data. STDS, South Tibetan Detachment System; LF, Lhunze Fault; GCT, Great Counter Thrust and IYR, Indus-Yarlung River. MFT, MBT, MCT, KT (Kakhtang thrust) and STDS attitude from Grujic *et al.* (2002) and McQuarrie *et al.* (2008); Tethyan Himalayan (I-I') features from Figure 3 (this study).

crosses out perpendicular to the main east–west trend of the belt, where little work has been done until now (Fig. 1b, c).

The present work combines the analysis of anisotropy of magnetic susceptibility (AMS) and structural data. The usefulness of AMS has been widely proved for studying deformation in weakly

deformed rocks like mudstones or granites with an incipient deformation (e.g. Borradaile & Tarling 1981; Tarling & Hrouda 1993; Bouchez 1997; Borradaile & Jackson 2004; Román-Berdiel *et al.* 2004). Moreover in deformed rocks, with a dominant paramagnetic signal of the tensor, AMS can be a reliable and fast tool for quantifying the

preferred orientation of elongated particles or structural elements or crystallographic alignment of minerals (e.g. Hirt *et al.* 1988; Averbuch *et al.* 1992; Parés & van der Pluijm 2002; Oliva-Urcia *et al.* 2009). The study of AMS in slightly deformed rocks has been recently emphasized by Burmeister *et al.* (2009) and it seems that it is able to highlight strain distributions more efficiently than measurements techniques of finite strain analyses.

### Major Himalayan tectonic elements

The Himalayan belt is the result of the complex superposition of two main tectonic and metamorphic phases: the Eohimalayan phase related to the first stages of the collision (Middle Eocene–Late Oligocene) and the Neohimalayan phase responsible for the main structure of the orogen (Early Miocene–present) (Hodges 2000; Fig. 2). Looking at the major Neohimalayan tectonic elements the Himalaya can be divided into four litho-tectonic units (Fig. 1b, c) (Gansser 1964; Le Fort 1975; Hodges 2000; Yin 2006). These are, from bottom to top and from south to north:

- (1) The Siwalik molasses in the footwall of the Main Boundary Thrust (MBT) made up of Himalayan foreland basin sediments of Miocene to Pliocene–Pleistocene age (Gansser 1964) (Fig. 1b, c).
- (2) The Lesser Himalayan Sequence (LHS) in the footwall of the Main Central Thrust (MCT) (Fig. 1b, c), consisting of sediments from Proterozoic to Cambrian reaching the Paleocene age in the more eastern sectors of the belt (Stöcklin 1980; Valdiya 1980). Sediments were deposited in a proximal position on the Indian shelf and deformed by thrusts and folds under very low-grade metamorphic conditions (Colchen *et al.* 1986; Hodges 2000).
- (3) The Greater Himalayan sequence (GHS) cropping out between the MCT and the set of north-dipping normal faults of the South Tibetan Detachment System (STDS) (Pécher 1991; Burchfiel *et al.* 1992). It represents the metamorphic core of the Himalayas with high grade metasediments and meta-igneous rocks (Le Fort 1975; Grujic *et al.* 2002). Leucogranitic intrusions are common in the contact zone with the STDS, for example, the Manaslu granite (e.g. Guillot *et al.* 1993). The contemporaneous activity of the MCT and the STDS, confined between 23–17 Ma (Godin *et al.* 2006) led to the exhumation of the GHS (Figs 1b, c & 2).
- (4) The Tethyan Himalaya sequence (THS) is a typical passive margin sequence deposited

on the Indian passive margin. It crops out between the south-dipping Great Counter Thrust (GCT) in the north and the STDS in the south (Fig. 1b, c). The Great Counter Thrust is a south-dipping thrust system (Heim & Gansser 1939; Searle 1986; Ratschbacher *et al.* 1994; Ding *et al.* 2005) which can be detected along the entire Himalaya from Zaskar to east of Gyaca (Fig. 1). North of the Great Counter Thrust the Indus Yarlung Suture Zone (IYSZ) marks the contact with the southern margin of Eurasia represented by the Lhasa Block. Moreover the Tethyan Himalayan sequences are affected by an Oligocene–Miocene discontinuous belt of metamorphic rocks and leucogranitic bodies named the North Himalayan gneiss domes (e.g. Hodges 2000; Lee *et al.* 2000).

### The Tethyan Himalayan Sequence, deformation and metamorphism

The Tethyan Himalayan Sequence crops out along c. 150 km between the South Tibetan Detachment System and the Indus Yarlung Suture Zone with approximately the same width from Annapurna to the East of Khula Kangri (Fig. 1b). The Tethyan Himalaya is built up of a continuous sedimentary sequence ranging from Cambro-Ordovician to Eocene and deposited on the passive northern margin of the Indian continent (Fuchs 1967; Willems *et al.* 1996; Garzanti 1999; Dupuis *et al.* 2006). The central Tethyan Himalaya can be divided in two sub-zones which are separated by the Gyrong-Kangmar Thrust (Liu 1992; Liu & Einsele 1994; Willems *et al.* 1996). The southern sub-zone is formed by slightly metamorphosed carbonate platforms and the northern sub-zone is defined by clastic sediments indicating the separation of the Indian plate from Gondwana and the following abyssal sedimentation conditions (Gaetani & Garzanti 1991; Brookfield 1993; Liu & Einsele 1994; Willems *et al.* 1996).

The sequence has experienced a complex structural history (see Fig. 2 for correlation of tectonic features in the Tethyan Himalaya). Godin (2003) defined five main phases of deformation, in the south Tethyan Himalaya in central Nepal, which can be partially or completely recognized along strike of the THS (Fig. 2). The first phase (D1) is defined by south-vergent small-scale folds (F1) with related low-grade axial planar foliation (S1) (e.g. Godin 2003; Carosi *et al.* 2007; Fig. 2). The D2 phase is characterized by large asymmetrical north-vergent megascopic backfolds (Kellett & Godin 2009) and a penetrative axial plane foliation (S2) defined by the preferred orientation of biotite,

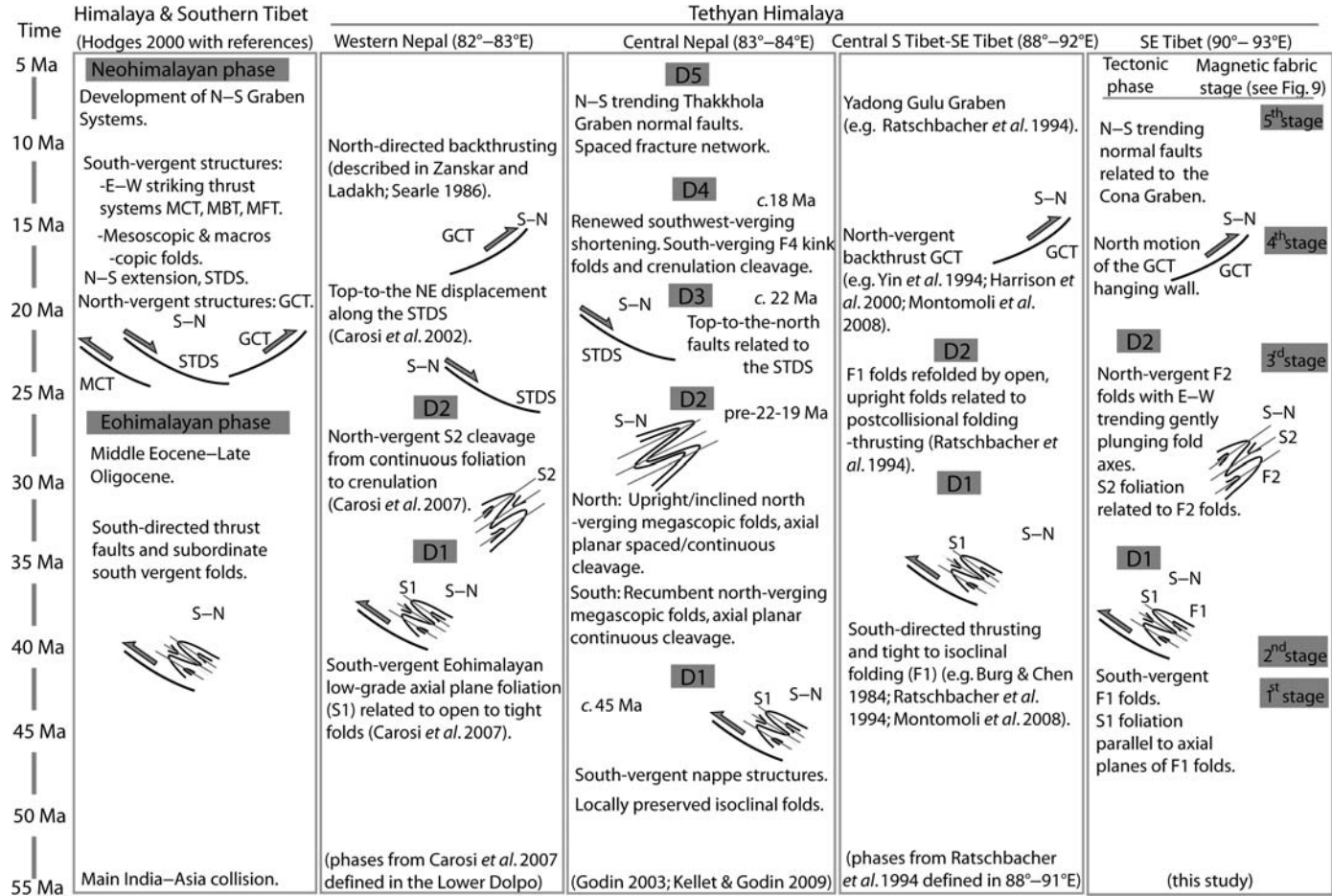


**Fig. 2.** Simplified synthesis of main deformation events in the Tethyan Himalaya from west to east. Left column refers to previous synthesis proposed by Hodges (2000) including general Himalayan events.

muscovite and elongated quartz grains in pelitic layers (Godin 2003; Carosi *et al.* 2007; Fig. 2). Crouzet *et al.* (2007) found K/Ar ages around 30–25 Ma interpreted as ages of recrystallized K-white micas newly formed during metamorphism and D2 in central Nepal. Moreover secondary pyrrhotite remanences show that F2 folding took place about 35–32 Ma (Appel *et al.* 1991; Crouzet *et al.* 2001; Schill *et al.* 2003). The third phase is related to the development of the South Tibetan Detachment system at *c.* 23–17 Ma for the whole belt (Godin *et al.* 2006 and references therein; Fig. 2). In the eastern Himalaya near Khula Kangri (Fig. 1b), Edwards & Harrison (1997) found an age <12.5 Ma for the STDS development. D4 deformation phase is characterized by SW–NE shortening recorded in post-peak metamorphic F4 kink folds associated with a regional crenulation cleavage S4 and SW directed thrusts (Godin 2003). Since at least the late Miocene (*c.* 8 Ma) east–west extension affected the Tethyan Himalaya sequence (D5 phase; Fig. 2) giving rise to north–south Graben structures, for example, the Takkhola Graben in central Himalaya and the Cona Graben in the eastern Himalaya (Armijo *et al.* 1986; Garzzone *et al.* 2003). The Tethyan Himalaya sequence experienced low-grade metamorphic conditions (Garzanti *et al.* 1994; Crouzet *et al.* 2007; Aikman *et al.* 2008; Dunkl *et al.* 2008) characterized by peak palaeotemperatures ranging from 250–450 °C (Crouzet *et al.* 2007). The age of the metamorphism decreases from the west to the east Himalaya ranging from 44–47 Ma in Zanskar to 30–25 Ma in central Himalaya (Bonhomme & Garzanti 1991; Crouzet *et al.* 2007).

### Study area: the Triassic flysch of the eastern Tethyan Himalaya

The present study is focused on the Triassic flysch of the Tethyan Himalaya with a sedimentation age of Middle Triassic to Early Jurassic (Chang 1984; Pan *et al.* 2004). Our work is concentrated in an area geographically located south of the Yarlung Tsangpo River that extends from Nagarze in the west as far as east of Gyaca (Fig. 3). Here the flysch consists of turbidites and carbonate flysch (Dupuis *et al.* 2005) and it is represented by black shales interbedded with sandstone/siltstone and locally some limestone. The organic-rich pelitic lithologies always contain early diagenetic pyrite crystals. The sequence is intruded by mafic dykes and contains small ultramafic intrusions. The dominant structures are folds and imbricate thrusts involving the whole passive continental margin sequence of the Tethyan Himalaya (Yin & Harrison 2000; Aikman *et al.* 2008).

In the north the Great Counter Thrust separates the Triassic flysch from the *mélange* complex and the Cretaceous clastic rocks (Fig. 3). The *mélange* complex (constituted by cherts, shales, marbles, andesites, diorites, mafic and ultramafic bodies, limestones and phyllites) has been deposited on the growing Neo-Tethys ocean floor and incorporated in a subduction complex *mélange* (Searle 1986). The Cretaceous clastic rocks were deposited in the active palaeomargin of the Indus Yarlung Suture Zone (Harrison *et al.* 2000; Pan *et al.* 2004; Dupuis *et al.* 2005). In the eastern Himalaya the Renbu-Zedong Thrust (Yin *et al.* 1994; Harrison *et al.* 2000) has been correlated with the Great Counter Thrust. The Great Counter Thrust in the Ringbung area is dated by K/Ar in a phyllite as 17.5 Ma old (Ratschbacher *et al.* 1994). This age coincides with the interval of activity from 18–10 Ma of the Great Counter Thrust in the Zedong area dated by Ar/Ar analyses on K-feldspar analysis (Quidelleur *et al.* 1997; Harrison *et al.* 2000).

Towards the south the Triassic flysch is in contact with the Upper Jurassic (continental clastic rocks, marls and marine limestones) and Cretaceous clastic rocks which represent the platform sequence of the Indian passive margin (e.g. Liu & Einsele 1996). The southern contact between the Triassic flysch and the Jurassic–Cretaceous rocks (Fig. 3) is marked by the Lhunze Fault which is likely comparable with the east–west-trending and north-dipping Gyrong-Kangmar Thrust cropping out around 50 km west of the Yadong Gulu Graben (Chen *et al.* 1990; Liu 1992; Yin 2006; Aikman *et al.* 2008).

Two kinds of intrusions have affected the Triassic flysch in the study area: the Dala granitoids of Eocene age (Aikman *et al.* 2008) and the Neogene North Himalayan gneiss domes (Fig. 3). The latter are represented by the Mt. Jangsang Lhamo south of Nagarze and the Yala Xiangbo south of Qusum (Fig. 3). Preliminary thermochronological data indicate that the Yala Xiangbo leucogranite was emplaced at *c.* 18 Ma, and cooled through the muscovite closure window at *c.* 13.5 Ma (Aikman *et al.* 2004; Zhang *et al.* 2005). The Neogene domes have been interpreted as metamorphic core complex owing to the fact that the granites are surrounded by detachment faults and shear zones (e.g. Zhang *et al.* 2005). Afterwards the east–west Neogene extension played a key role in the deformation of the eastern Tethyan Himalaya giving rise to the NNE–SSW Cona Graben that can be followed from the north of the Indus Yarlung Suture Zone as far as the South Tibetan Detachment System, with *c.* 210 km length and 8 km width (Fig. 3). The Cona Graben is the easternmost graben that crosses the Tethyan Himalaya and GPS velocities

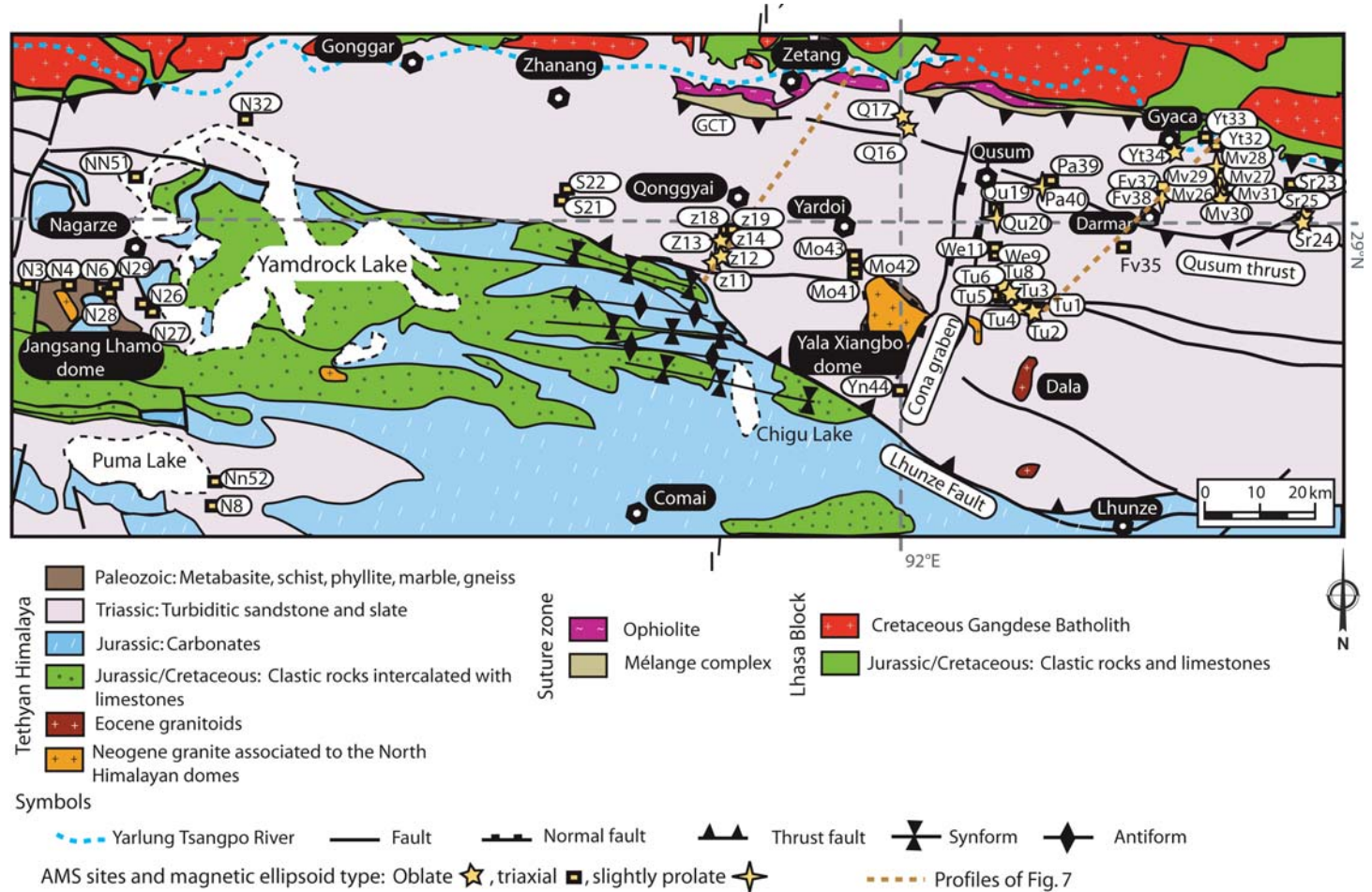


**Fig. 3.** Simplified geological map of SE Tibet. Modified from Pan *et al.* (2004), Yin (2006) and Aikman *et al.* (2008). The studied sites are marked in function of the type of AMS ellipsoid. Line I-I' indicates the cross-section in Figure 1c. Dashed orange lines indicate the two cross-sections of Figure 7.

have indicated no significant ( $0.3 \pm 0.9 \text{ mm a}^{-1}$ ) fault opening at present-day (Gan *et al.* 2007).

### Structural and metamorphic data

A polyphase tectonic history has been recognized in the study area characterized by two main tectonic phases named hereafter D1 and D2 (see Fig. 2 for correlation between Tethyan Himalayan deformation phases). During the first D1 tectonic phase, referred to the Eohimalayan event (Hodges 2000), metric to kilometric asymmetrical F1 folds developed. F1 folds face to the south and their axes trend ENE–WSW. Parallel to axial planes of F1 folds, a S1 axial plane foliation can be recognized (see stereograms of sector 1, south of sector 2 and sector 3 in Fig. 4a). In the southern parts of the studied area S1 is the dominant planar structure in the field (Fig. 4b). In the Nagarze area (sector 1; Fig. 4a) the mean vector of the S1 poles trends  $220^\circ$  and plunges  $70^\circ$  ( $\alpha_{95} = 22^\circ$ ;  $k = 4.9$ ) and in the Qonggyai valley (south of Zetang in sector 2; Fig. 4a) the S1 pole mean vector trends  $182^\circ$  and plunges  $30^\circ$  ( $\alpha_{95} = 24^\circ$ ;  $k = 13.8$ ; Fig. 4a). East of the Cona Graben, in sector 3, S1 poles mean vector trends  $210^\circ$  and plunges  $35^\circ$  ( $\alpha_{95} = 5.6^\circ$ ;  $k = 7.3$ ; Fig. 4c). S1 is a low grade foliation and microstructural observations show that moving from south to north, S1 foliation varies from a disjunctive spaced stylolitic cleavage with no dynamic recrystallization to a fine continuous foliation (Montomoli *et al.* 2008) marked by syn-kinematic recrystallization of very fine-grained phyllosilicates (Fig. 4d). Object lineations, trending NW–SE, are well represented by strain fringes, mainly composed of quartz around pyrite crystals. D1 deformation occurred in diagenetic or lower anchizonal conditions probably in Paleogene times (Dunkl *et al.* 2008).

A later D2 deformation phase is superimposed on D1 structures (Fig. 2). D2 is represented by a weak crenulation cleavage in the southern portions but moving towards the GCT it gives rise to decimetre to decametre-scale F2 folds (Fig. 4e). F2 folds have east–west-trending gently plunging axes and verge to the north. Associated with F2 folds a S2 foliation was generated. Axial plane foliation S2 strikes WNW–ESE with moderate dips towards the south (see stereograms north of sector 2 and sector 4 in Fig. 4a). Equal area projection of S2 poles of sector 4 show a grouping ( $\alpha_{95} = 14.6^\circ$ ;  $k = 3.2$ ; Fig. 4c) with a mean vector trending  $007^\circ$  and plunging  $43^\circ$  (Fig. 4a, c). Foliation S2 varies from a discrete zonal crenulation with well defined cleavage domains near the Qusum Thrust (Fig. 4f) to a fine continuous foliation in a more strained area in the vicinity of the Great Counter Thrust,

where S2 is the most visible structural element in the outcrop. In some cases, in the more northern areas S2 is associated with the dynamic recrystallization of illite-sericite (Montomoli *et al.* 2008). East of the Cona Graben the WNW–ESE-trending thrust fault with south to south–SW dip described in Yin (2006), that we name the Qusum Thrust, represents the boundary between S1 and S2 foliations.

Top-to-the-N or NE brittle–ductile shear zones are developed in the overturned limbs of F2 folds with kinematic indicators such as C–S fabric (Berthé *et al.* 1979). On C surfaces stretching lineations strike north–south and plunge gently to the south (Montomoli *et al.* 2008; see Fig. 4a stereogram with stretching lineation within S2 at site Yt32). D2 took place at higher anchizonal to greenschist facies conditions in Miocene times and the process culminated around 24 Ma as Dunkl *et al.* (2008) have shown.

### AMS analysis

AMS was measured in 516 cylindrical rock specimens with a standard size of 2.5 cm diameter and 2.1 cm length. Samples were collected from 53 sites distributed along north–south valleys between Yamdrock lake and east of Gyaca (Fig. 3), with an average of 10 cores at each site. A portable gasoline powered rock drill machine was used and cores were oriented *in situ* with a magnetic compass. The study of AMS was carried out with an AGICO KLY-2 Kappabridge at Tuebingen University. The AMS ellipsoid was determined from 15 different directional measurements. The results can be characterized by the bulk susceptibility ( $K_m$ ) given as arithmetic mean of the three principal axes of the AMS ellipsoid:  $K_m = 1/3(K_{\max} + K_{\text{int}} + K_{\min})$  and the orientations and magnitudes of the  $K_{\max} > K_{\text{int}} > K_{\min}$  axes of the AMS ellipsoid. The statistical procedure to obtain the directional data was based on tensor analysis by Jelinek (1977), using the program anisoft42 developed by Chadima and Jelinek (last version of 2008). The mean values for areas were calculated by Fisher statistics (Fisher *et al.* 1987) with the program Stereogram v. 1.2 (R. Allmendinger). In numerous tectonic and AMS studies it has been shown that in rocks where iron-rich silicates control magnetic susceptibility the cluster of minimum axes of the magnetic ellipsoid ( $K_{\min}$ ) is related to the magnetic foliation because the minimum susceptibility axis is nearly perpendicular to the basal cleavage of phyllosilicates crystals (e.g. Kneen 1976; Borradaile & Werner 1994; Martín-Hernández & Hirt 2003). A cluster of maximum axes ( $K_{\max}$ ) or magnetic lineation can reflect either the extension direction, the intersection of two competing subfabrics (because the

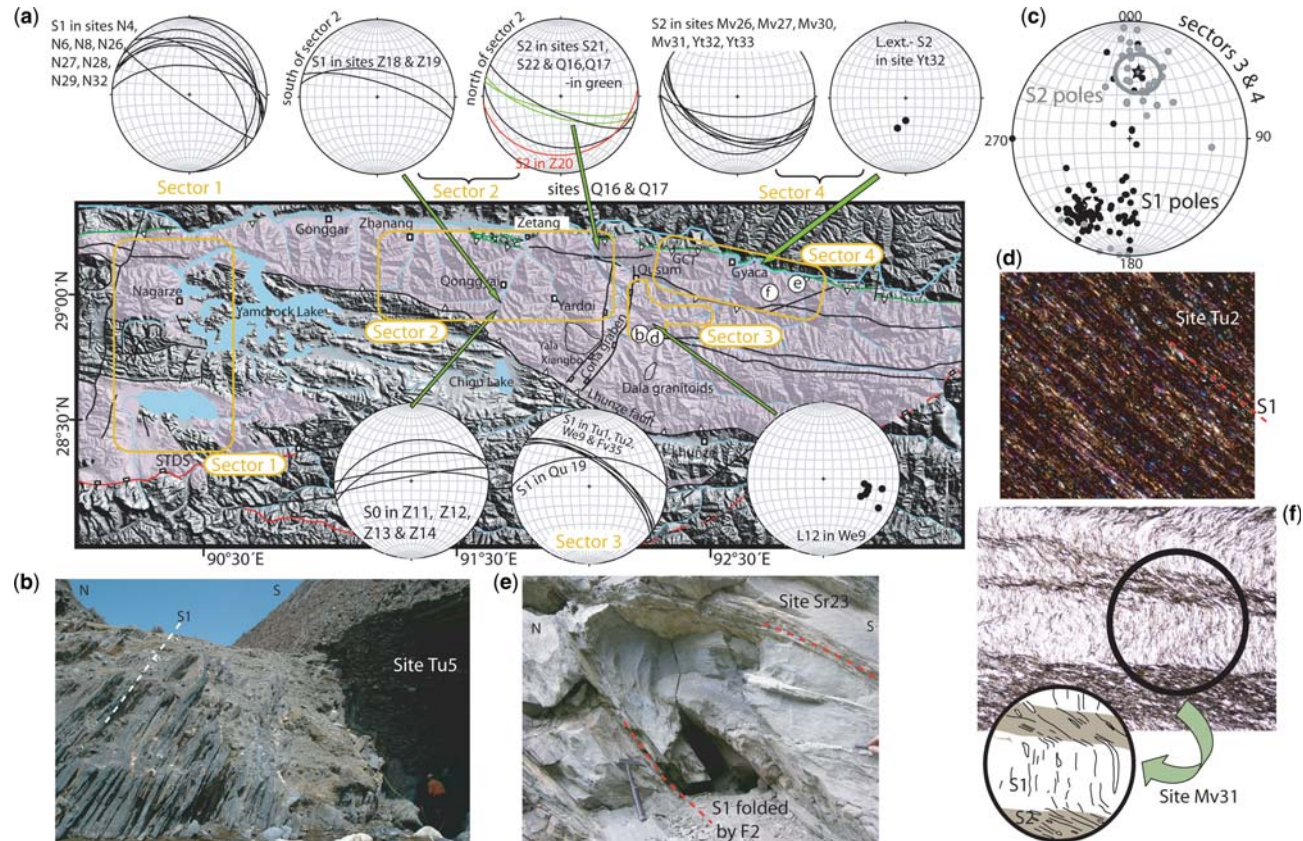


**Fig. 4.** (a) SRTM topography overlapped with the Triassic flysch (pink colour) and the structural elements of Figure 3. The orange rectangles show the sectors described in the structural and magnetic fabric sections; b, d, e and f letters correspond to the position of the outcrop and thin section images. Lower-hemisphere, equal-area stereogram of the general trend of tectonic foliations per site and stretching lineation (L.ext.) within S2 foliation from site Yt32 and intersection lineations of foliation S1 and S2 (L12) in site We9. (b) Outcrop view of site Tu5, dashed line shows S1 foliation. (c) Lower-hemisphere, equal-area stereogram of the poles of S1 and S2 tectonic foliations of sector 3 and 4, stars indicate mean vectors. (d) Photomicrograph of S1 foliation developed in the slates of the site Tu2 (field of view 5 mm). (e) Example of F2 fold in site Sr23. (f) Thin section photomicrograph from the slates of the site Mv31 and geological interpretation; both S1 and S2 foliations are recognizable (field of view 7 mm).

maximum susceptibility axis is the intersection axis between the phyllosilicates crystals), or an orientation in between (Borradaile & Tarling 1981; Housen *et al.* 1993; Parés *et al.* 1999; van der Pluijm 2002; Soto *et al.* 2003).

Furthermore Jelinek's method gives different scalar parameters which are very useful to describe the magnetic fabrics: the corrected anisotropy degree ( $P'$ ) can be related to the intensity of the preferred orientation of minerals in rocks in which the susceptibility is mainly carried by paramagnetic minerals. The shape parameter ( $T$ ) indicates the form of the magnetic ellipsoid.  $T$  can range from  $-1$  (prolate ellipsoid) to  $1$  (oblate ellipsoid). The magnetic foliation parameter ( $F = K_{\text{int}}/K_{\text{min}}$ ) and magnetic lineation parameter ( $L = K_{\text{max}}/K_{\text{int}}$ ) can be plotted in a Flinn type plot (Flinn 1962) normally used in structural geology. We used also Jelinek's elliptical confidence angles as markers of the quality of AMS data (Jelinek 1977).

### *Magnetic mineralogy and carriers of the magnetic fabric*

The determination of the minerals that contribute to the anisotropy of magnetic susceptibility is an essential step in order to understand the origin of the magnetic fabric and their structural interpretation. In the following we predominantly utilize median values and quartiles for concentration-dependent parameters because these are more representative that mean values and standard deviation in data sets with some significant outliers.

The bulk susceptibility median of the 53 studied sites is  $232 \times 10^{-6}$  SI (1st quartile =  $187 \times 10^{-6}$  SI, 3rd quartile =  $372 \times 10^{-6}$  SI, mean =  $334 \times 10^{-6}$  SI and STD =  $314 \times 10^{-6}$  SI) (Table 1; Fig. 5a). Around 89 % of the sites show a low bulk susceptibility median  $< 500 \times 10^{-6}$  SI typical for rocks where the magnetic fabric is usually controlled by the crystal lattice orientation of the paramagnetic fraction (Rochette 1987). Similar values of magnetic susceptibility have been found in other studies where paramagnetic minerals controlled the AMS ellipsoid (e.g. Tarling & Hrouda 1993). Sites N6, Tu5, Tu6 and Mv30 have higher values ( $K_m > 800 \times 10^{-6}$  SI) probably related to a significant contribution of the ferro(i)magnetic fraction to the total magnetic susceptibility and they will be analysed separately. Natural Remanent Magnetization (NRM) was measured in 10 samples per site with a 2 G RF-SQUID magnetometer. The NRM median is low, 0.4 mA/m (1st quartile = 0.26 mA/m, 3rd quartile = 1.4 mA/m, mean = 10.8 mA/m and STD = 43.3 mA/m) (Table 1). Around 72% of the sites give median values of NRM  $< 1$  mA/m and there is no

correlation of  $K_m$  and NRM ( $R^2 = 0.12$ ) likely indicating a low content of ferro(i)magnetic minerals (Fig. 5a). A similar analysis was carried out on 41 samples from 24 sites, looking at the relation between the  $K_m$  and saturation isothermal remanent magnetization (SIRM) at 2.4 T (SIRM imparted by a MMPM9 pulse magnetizer). Also for SIRM and  $K_m$  no significant dependence was found. Variation of magnetic susceptibility was measured for 14 sites between  $-196^\circ\text{C}$  and room temperature using a low temperature unit attached to a KLY-3 Kappa-bridge (AGICO). The measured thermomagnetic curves, after free furnace correction, show a temperature dependence of susceptibility following the Curie Law (Nagata 1961) characteristic for paramagnetic minerals (Fig. 5b). Moreover variation of magnetic susceptibility was measured for 7 sites between room temperature and  $700^\circ\text{C}$  using a high temperature unit attached to a KLY-3 Kappa-bridge (AGICO). The measured thermomagnetic curves, after free furnace correction, show no presence of pyrrhotite and a minor contribution of magnetite indicated by decay around  $580^\circ\text{C}$ .

In thin sections and in outcrop views we observed pyrite crystals inside the slates. Pyrite influence on the total magnetic susceptibility is small but it is an important source for the creation of pyrrhotite during the metamorphism (Rochette 1987; Borradaile & Sarvas 1990; Crouzet *et al.* 2001). The main decay of intensity of the SIRM around  $325^\circ\text{C}$  indicates the presence of pyrrhotite in all the studied samples (Fig. 5c). IRM acquisition in a direct field up to a maximum of 1.8 T shows near saturation at 0.3 T suggesting that the pyrrhotite grains are in a rather low coercive multidomain state. It is also noted that in site Yt32 additional magnetite was observed by its Curie temperature around  $580^\circ\text{C}$ .

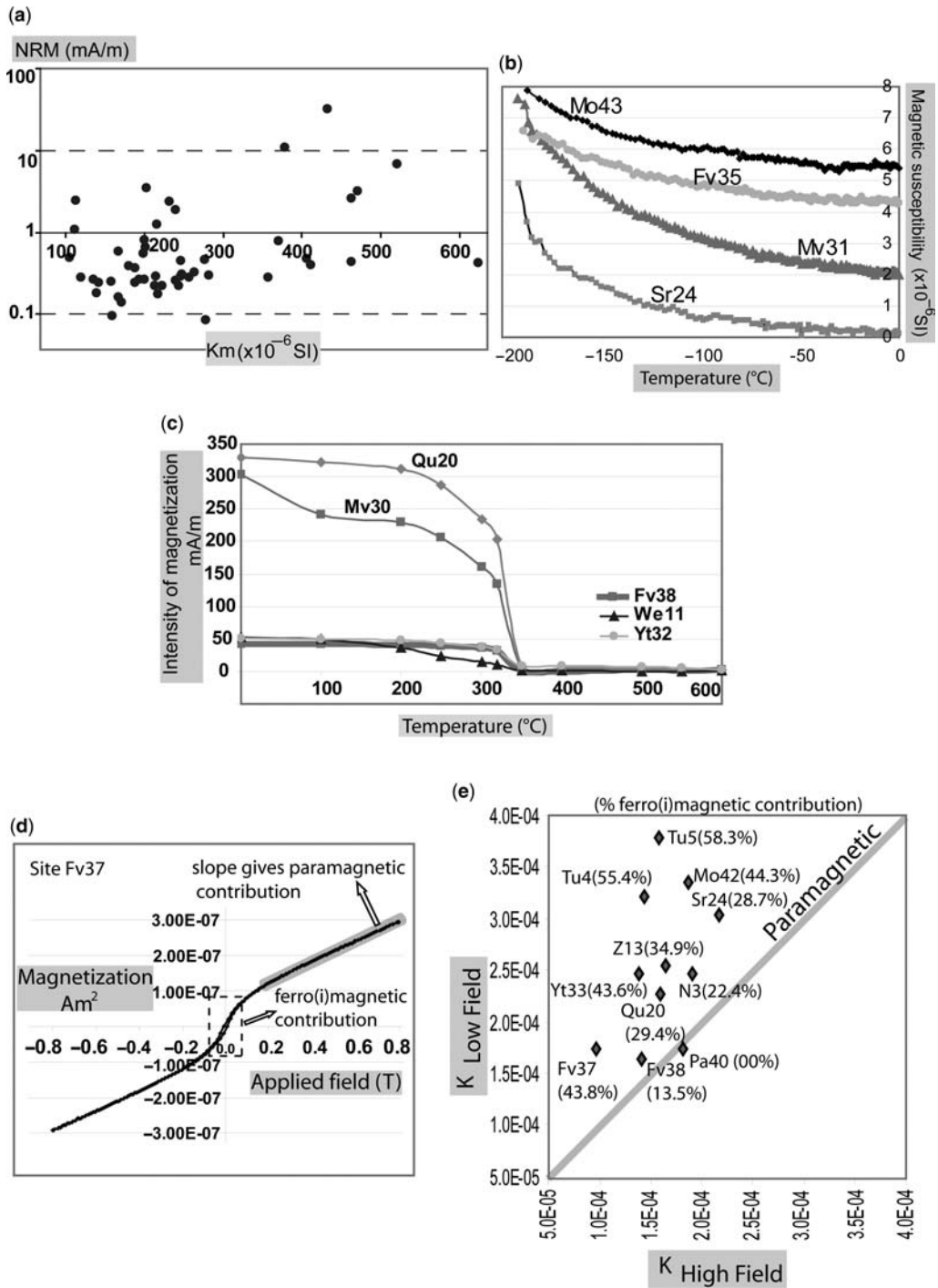
The aforementioned results were further examined quantitatively by means of hysteresis properties. Hysteresis properties were measured in 28 sites with an Alternating Gradient Force Magnetometer AGFM 2900 (Princeton Measurements Corp.). The maximum applied field was 800 mT in which the ferro(i)magnetic phase is fully saturated. All samples show a straight line at high fields due to the intrinsic high field susceptibility of the paramagnetic minerals (Borradaile & Werner 1994). The ferro(i)magnetic component shows a low coercivity ( $H_c < 10$  mT) confirming the presence of a very low coercive MD pyrrhotite or some contribution of magnetite (Fig. 5d). In order to quantify the paramagnetic and ferro(i)magnetic contribution to the total magnetic susceptibility we calculated the bulk specific susceptibility of the paramagnetic fraction from the slope of the hysteresis loop at high fields and compared it with the total bulk specific susceptibility at low fields of the same sample as

Table 1. NRM and AMS data

Site	NRM (mA/m)	n	AMS type	Km (*10E-6 SI)	K <sub>max</sub> (T/P)	CA	K <sub>min</sub> (T/P)	CA	P'	T
<b>Tu1</b>	28.44 ± 21.10	16	2	432.8 ± 372.8	114/30	26/6	215/18	15/6	1.56	0.65
<b>Tu2</b>	0.35 ± 0.18	12	2	180.4 ± 50.6	314/20	60/11	217/17	15/8	1.23	0.82
<b>Tu3</b>	64.18 ± 115.6	8	1	463.0 ± 797.1	121/17	36/6	223/35	8/4	1.41	0.74
<b>Tu4</b>	0.33 ± 0.28	11	1	239.5 ± 39.7	310/10	31/8	215/27	14/7	1.28	0.94
<b>Tu5</b>	349.6 ± 269.6	10	2	1395.0 ± 1079.0	345/44	30/18	212/35	22/10	2.12	0.44
<b>Tu6</b>	98.85 ± 121	10	2	1304 ± 1079.0	342/47	22/12	210/31	14/7	2.08	0.59
<b>Tu8</b>	11.95 ± 14.48	10	1	239.7 ± 38.3	310/18	19/6	215/14	36/17	1.24	0.60
<b>We9</b>	9.04 ± 12.23	10	2	470.7 ± 198.7	113/22	12/6	217/31	17/6	1.30	0.43
<b>We11</b>	23.63 ± 58.19	10	1	623.5 ± 467.0	082/33	13/5	207/42	7/5	1.54	0.61
<b>Qu19</b>	0.29 ± 0.11	11	2	246.8 ± 23.8	284/9	14/5	187/34	9/3	1.17	0.30
<b>Qu20</b>	0.78 ± 0.63	9	3	214.4 ± 15.8	280/9	19/14	168/67	27/11	1.16	-0.13
<b>Sr23</b>	0.34 ± 0.36	9	2	243.7 ± 99.3	277/11	12/4	014/33	12/5	1.15	0.61
<b>Sr24</b>	0.58 ± 0.37	7	1	166.8 ± 45.1	103/15	81/17	003/33	19/7	1.15	0.59
<b>Sr25</b>	0.84 ± 1.09	10	1	105.3 ± 38.8	124/19	39/7	019/38	8/6	1.17	0.70
<b>Mv26</b>	0.61 ± 0.25	9	1	199.7 ± 73.1	140/12	49/13	031/57	30/18	1.21	0.30
<b>Mv27</b>	0.49 ± 0.15	7	3	276.5 ± 27.5	262/29	8/6	004/19	34/5	1.16	0.09
<b>Mv28</b>	0.33 ± 0.18	9	1	357.1 ± 83.4	141/65	34/15	032/9	15/12	1.26	0.58
<b>Mv29</b>	0.45 ± 0.24	13	3	411.6 ± 69.0	271/9	12/10	179/13	36/7	1.18	0.14
<b>Mv30</b>	157.7 ± 184.80	13	1	1684 ± 1521.0	167/44	48/11	014/43	13/6	2.35	0.39
<b>Mv31</b>	22.56 ± 28.78	10	3	520.7 ± 477.8	285/14	9/4	188/25	47/9	1.46	-0.07
<b>Yt32</b>	0.54 ± 0.91	9	2	282.1 ± 42.2	193/70	10/4	003/20	11/4	1.18	0.61
<b>Yt33</b>	0.49 ± 0.30	10	2	246.2 ± 23.5	189/64	24/16	030/24	23/15	1.37	0.85
<b>Yt34</b>	23.97 ± 35.00	9	1	377.8 ± 277.2	109/24	56/7	006/26	8/5	1.38	0.40
<b>Fv35</b>	1.66 ± 1.29	10	2	216.1 ± 51.0	122/7	33/5	216/28	7/5	1.16	0.54
<b>Fv37</b>	0.01 ± 0.05	7	2	160.0 ± 20.9	149/48	20/4	024/27	7/4	1.28	0.70
<b>Fv38</b>	0.47 ± 0.55	11	3	119.6 ± 27.6	281/2	14/6	015/68	22/6	1.15	0.43
<b>Pa39</b>	0.30 ± 0.14	10	2	247.3 ± 105.4	091/36	28/15	190/13	19/14	1.28	0.58

<b>Pa40</b>	0.13 ± 0.06	11	3	171.6 ± 43.9	283/6	15/6	125/83	39/10	1.23	0.49
<b>N3</b>	10.20 ± 18.34	14	1	370.0 ± 277.0	298/3	13/4	095/86	5/3	1.20	0.44
<b>N4</b>	45.64 ± 106.60	11	1	203.0 ± 178.0	332/8	4/3	161/82	6/2	1.33	0.50
<b>N6</b>	216.70 ± 357.90	14	2	857 ± 702.0	344/13	4/2	198/75	3/1	2.29	0.02
<b>N8</b>	1.13 ± 2.35	9	1	264.0 ± 38.5	298/14	25/1	143/74	7/2	1.15	0.61
<b>N26</b>	3.08 ± 2.12	12	2	232.0 ± 38.4	331/50	12/6	177/37	10/3	1.15	0.65
<b>N27</b>	1.22 ± 1.45	11	2	112.0 ± 28.5	297/66	6/3	205/1	8/3	1.17	0.68
<b>N28</b>	3.03 ± 3.11	10	2	113.0 ± 14.5	329/33	8/5	215/32	7/3	1.17	0.63
<b>N29</b>	0.96 ± 0.55	9	2	200.0 ± 75.1	356/33	16/7	210/52	13/7	1.07	0.27
<b>N32</b>	0.35 ± 0.32	9	1	189.0 ± 30.5	123/24	58/28	220/15	30/17	1.07	0.31
<b>Nn51</b>	0.08 ± 0.04	5	2	278.0 ± 20.1	164/54	19/2	339/36	5/3	1.12	0.56
<b>Nn52</b>	1.84 ± 3.14	10	2	406.0 ± 77.4	339/30	10/4	211/47	20/3	1.12	-0.09
<b>Q16</b>	0.29 ± 0.22	10	1	167.0 ± 40.0	253/51	22/3	011/20	5/3	1.21	0.83
<b>Q17</b>	0.36 ± 0.43	7	1	140.0 ± 64.3	248/53	38/5	010/22	9/6	1.14	0.59
<b>S21</b>	0.26 ± 0.16	5	2	142.0 ± 17.5	219/22	11/1	350/58	15/2	1.05	0.37
<b>S22</b>	0.36 ± 0.23	8	2	189.0 ± 12.6	228/78	9/8	007/10	10/6	1.08	0.41
<b>Z11</b>	0.21 ± 0.08	10	1	213.0 ± 16.5	083/4	24/5	175/17	7/2	1.08	0.65
<b>Z12</b>	1.73 ± 3.32	11	1	194.0 ± 25.6	285/29	30/7	179/27	19/12	1.20	0.80
<b>Z13</b>	0.23 ± 0.29	11	2	223.0 ± 23.3	012/47	7/3	173/41	17/2	1.21	0.83
<b>Z14</b>	1.04 ± 0.95	10	1	202.0 ± 46.9	081/12	21/7	174/16	8/6	1.11	0.79
<b>Z18</b>	0.27 ± 0.25	12	2	136.0 ± 45.2	056/55	18/5	185/23	7/1	1.09	0.45
<b>Z19</b>	0.29 ± 0.20	12	2	158.0 ± 16.7	015/69	5/4	189/21	7/4	1.10	0.29
<b>Mo41</b>	3.40 ± 5.74	9	2	463.0 ± 291.0	348/40	11/3	160/50	6/3	1.07	-0.07
<b>Mo42</b>	0.28 ± 0.16	9	2	257.0 ± 22.9	005/43	10/5	157/44	10/3	1.19	0.68
<b>Mo43</b>	0.26 ± 0.36	10	2	218.0 ± 36.9	340/46	10/5	147/44	6/4	1.17	0.65
<b>Yn44</b>	0.27 ± 0.04	7	2	201.0 ± 10.3	279/16	11/3	169/50	10/4	1.07	0.28

NRM, natural remanent magnetization mean (mA/m); STD, Standard deviation. AMS data (Jelinek's statistics, 1977): n, number of measured samples; Km, Bulk magnetic susceptibility ( $\times 10^{-6}$  SI);  $K_{\max}$  and  $K_{\min}$  mean (trend/plunge) with the 95% confidence angle (CA). P', corrected degree of anisotropy; T, shape parameter.



**Fig. 5.** Magnetic mineralogy analysis. (a)  $K_m$  v. NRM plot without sites Tu5, Tu6, Mv30 and N6 with important ferro(i)magnetic contribution, see discussion in the text. (b) Curves of magnetic susceptibility v. the temperature. (c) Thermal demagnetization curves of the SIRM. (d) Hysteresis curve from site Fv37. (e) High field bulk magnetic susceptibility v. low field bulk magnetic susceptibility essays.

was previously done by other authors (e.g. Richter & van der Pluijm 1994). The values obtained in 11 samples from different homogeneously distributed sites indicate that in five samples (sites Pa40, Fv38, N3, Qu20, Sr24) the ferro(i)magnetic contribution is less than 30% and in six samples (sites Fv37, Z13, Yt33, Mo42, Tu4, Tu5) the ferro(i)magnetic contribution to the total magnetic susceptibility is in between 30% and 60% (Fig. 5e).

However, one has to be cautious with these results as they are based on very small samples and thus reliability of upscaling is dependent on the homogeneity of the rocks.

Consequently all these results in conjunction with the well defined magnetic foliation parallel to the tectonic foliation plane and the fact that  $P'$  values are characteristic of rocks governed by phyllosilicates (Fig. 6a) point out that a predominating

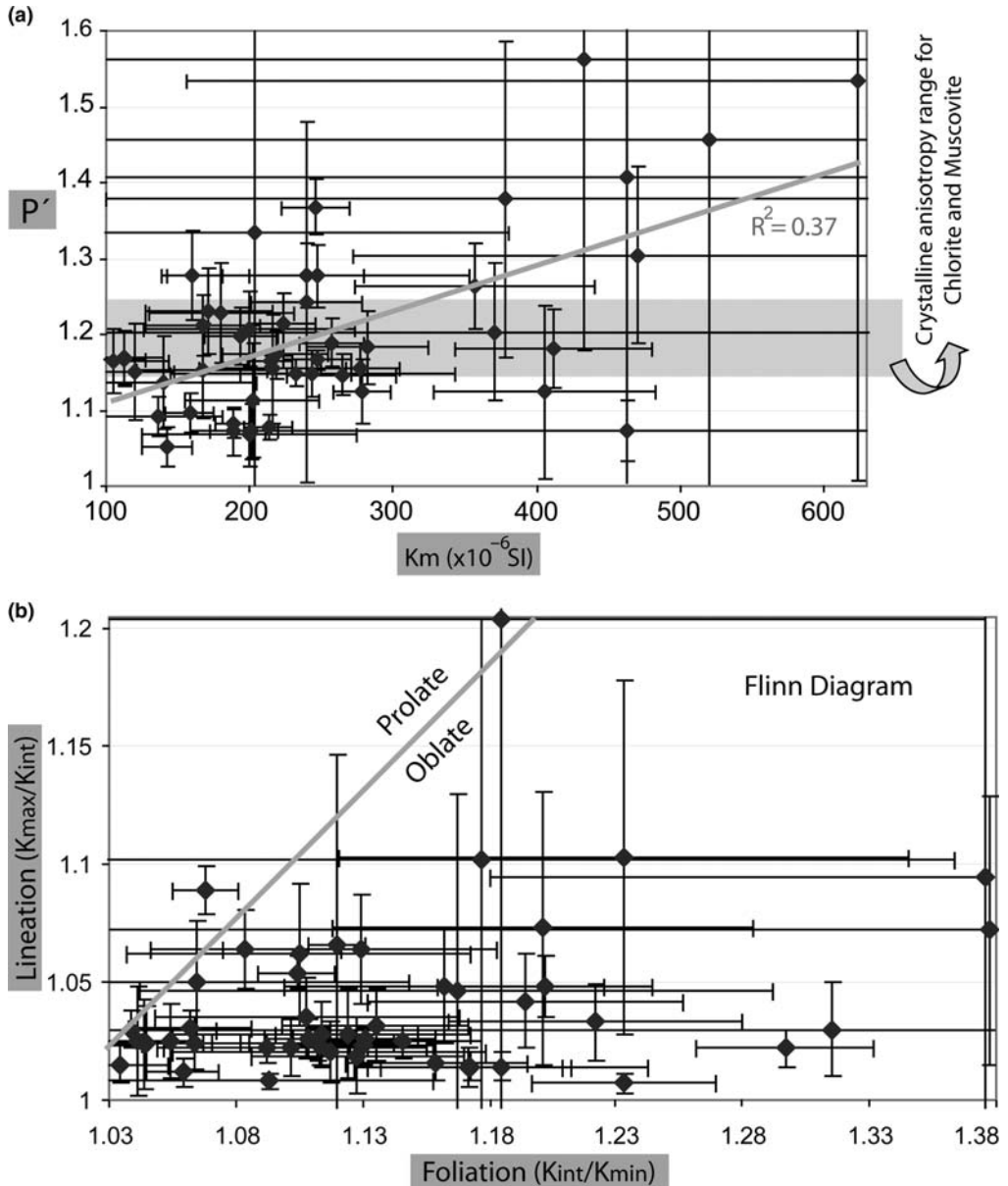


Fig. 6. AMS scalar parameters plots. (a)  $K_m$  v.  $P'$ . (b) Flinn diagram.

paramagnetic control of the total anisotropy of magnetic susceptibility can be expected in most sampled sites. For this reason the geographical distribution of the axes of the ellipsoid of magnetic susceptibility can be interpreted in terms of the preferred orientation of the phyllosilicates in relation to their structural location. However, there might be also some small contribution from subordinate pyrrhotite or magnetite mainly in sites Tu5, Tu6, Mv30 and N6 which have not been included in the scalar parameter plots and in the tectonic interpretation. Although these four sites show  $K_{\min}$  axis nearly perpendicular to the tectonic foliation (Table 1 & Fig. 4a) as in the sites controlled by the paramagnetic mineral fraction, may be related to a co-axiality of magnetic fabrics and petrofabrics, as was previously noted by Borradaile & Sarvas (1990) in the slates west of Atikokan (Canada).

#### *AMS ellipsoid: the corrected degree of anisotropy and shape parameters*

The corrected degree of anisotropy ( $P'$ ) in the slates of SE Tibet is in the range of  $P'$  characteristic for slates where the main carriers of the AMS are phyllosilicates (Tarling & Hrouda 1993; Parés & van der Pluijm 2002). The sites show a median value of 1.18 (1st quartile = 1.14; 3rd quartile = 1.27; Mean = 1.28, STD = 0.30) (Fig. 6a & Table 1). Moreover these values are similar to the crystalline anisotropies of chlorite ( $P' = 1.15-1.19$ ) or muscovite ( $P' = 1.15-1.27$ ) (values of  $P'$  given by Martín-Hernández & Hirt 2003 and Borradaile & Werner 1994 respectively). In order to detect the dependence of the corrected degree of anisotropy on the rock composition (iron content) we studied the relation between the corrected degree of anisotropy and  $K_m$  at site scale and regional scale. Only two sites (We9 and Sr23) indicate dependence of the corrected degree of anisotropy on the magnetic susceptibility at site scale. The plot of  $K_m$  v.  $P'$  mean site values indicates no correlation between the magnetic susceptibility (iron content) and the degree of anisotropy ( $R^2 = 0.37$ ; Fig. 6a). These data corroborate the magnetic mineralogy analysis suggesting that the phyllosilicates predominantly control the AMS signal.

The shape of the magnetic ellipsoid is oblate in 92% of the sites; only sites N6, Qu20, Nn52 and Mo41 show a slightly prolate ellipsoid. The shape parameter mean is 0.5 (STD = 0.26) suggesting the dominance of a planar fabric controlled by the foliation (Fig. 6b & Table 1). Likewise the  $F$  parameter ( $F$  mean = 1.18, STD = 0.16) and the  $L$  parameter ( $L$  mean = 1.06, STD = 0.08) distribution in the Flinn diagram confirms the control of the foliation (Fig. 6b).

#### *Different shapes of AMS ellipsoids, definition of magnetic foliation and lineation*

Equal area plots of the principal AMS axes show three typical shapes of AMS ellipsoids (Figs 3, 7 & Table 1). The first type is an oblate ellipsoid with a cluster of  $K_{\min}$  perpendicular to the foliation plane and  $K_{\max}$  and  $K_{\text{int}}$  distributed along the foliation plane (e.g. site Q16 in Fig. 7a). The fact that  $K_{\max}$  is not grouped prevents the definition of the magnetic lineation (e.g. Pueyo *et al.* 2004). The second type and most common one shows a triaxial ellipsoid with all three axes well grouped;  $K_{\min}$  axes are perpendicular to the foliation plane and  $K_{\max}$  axes represent different structural elements. They can be parallel to the F1 or F2 fold axes, related to the intersection of S1 and S2 as previously documented Housen *et al.* (1993) (e.g. see Fig. 4a intersection lineation of S1 and S2, L12, in site We9 is nearly parallel to  $K_{\max}$  orientation of We9; Table 1) or parallel to the stretching lineation (e.g. site Yt32 in Fig. 7b). The third type presents a slightly prolate ellipsoid characterized by a semi-girdle distribution of  $K_{\min}$  axes and a cluster of  $K_{\max}$  axes, magnetic lineation, which is related the intersection lineation of S1 and S2 foliations as can be seen in the site Qu20 in Figure 7b. How these ellipsoids are spatially distributed in the studied area as well as the orientation and relation with the structural elements is discussed below.

#### *Magnetic foliation and lineation in the Triassic flysch of SE Tibet*

Four sectors like in the structural section have been distinguished in order to understand the relation between the magnetic fabric and the structural data (Fig. 8).

Sector 1 mainly corresponds to the Nagarze area, which is located east of the Yadong Gulu Graben and in the vicinity of the Jangsang Lhamo North Himalayan gneiss dome (Figs 4 & 8). These nine sites show a triaxial magnetic ellipsoid described above. Magnetic foliation strikes WNW-ESE with moderate dips towards the north and parallel to S1 tectonic foliation (Fig. 8a). It is also noted that the dip varies from very gentle angles beside the Jangsang Lhamo Dome to near vertical moving to the east. Magnetic lineation has a NNW-SSE trend and north-NW plunge approximately parallel to gneiss dome elongation (Fig. 8b). Like the magnetic foliation the plunge values of the magnetic lineation increase from the Jangsang Lhamo dome to the east. Furthermore two sites were drilled in the east side of the Puma Lake and c. 40 km north of the South Tibetan Detachment System (Fig. 3; sites N7 and N8).

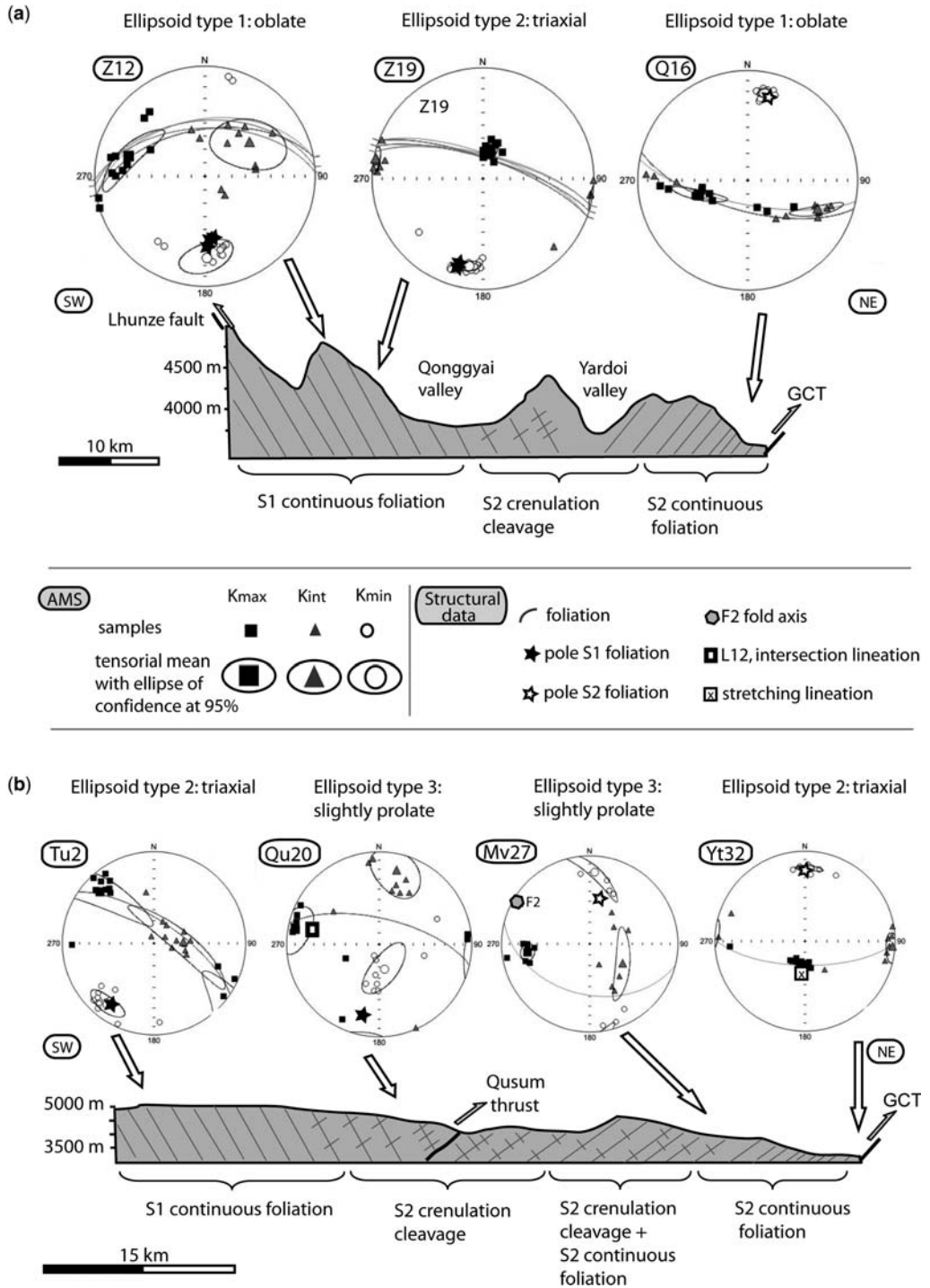


**Fig. 7.** Types of AMS ellipsoids within two simplified cross-sections indicated in Figure 3 with the schematic stages of cleavage development. (a) Cross-section from the Lhunze fault to the Great Counter thrust along the Qonggyai valley. (b) Cross-section crossing sectors 3 and 4.

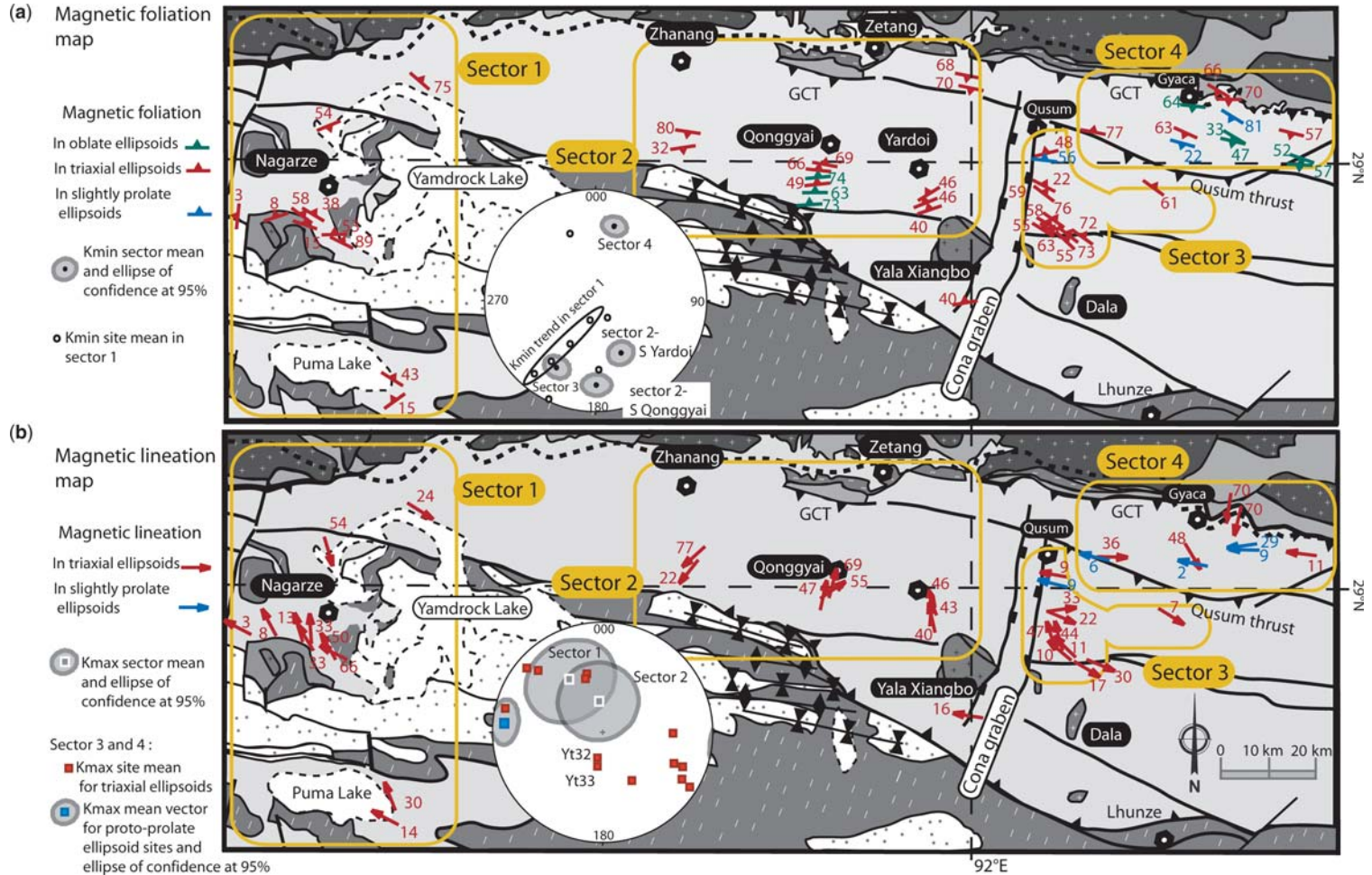


**Fig. 8.** (a) Magnetic foliation map and lower-hemisphere, equal-area stereogram with the  $K_{min}$  mean vector for sector 2 south of Yardoi, sector 2 south of Qonggyai, sector 3, sector 4 and scattered distribution of single sites  $K_{min}$  mean vector of sector 1. (b) Magnetic lineation map and lower-hemisphere, equal-area stereogram of  $K_{max}$  mean vector for sector 1 and 2, and  $K_{max}$  mean vector for sites within sectors 3 and 4. Both maps follow the same map legend of Figure 3 with greyscale colours.

These two sites have directions and plunges of the magnetic lineation and foliation that follow the general trend of the magnetic axes at Nagarze.

Sector 2 covers the valleys south of Zhanang and Zetang towards Yala Xiangbo dome (Figs 4 & 8). Sites S21 and S22 in the Zhanang valley present triaxial magnetic ellipsoids with magnetic foliation trending east–west with moderate dip to the south parallel to S2 tectonic foliation. Magnetic lineation trends NNE–SSW with plunge towards the south–SW. The Qonggyai profile (location in Fig. 3) presents AMS ellipsoids that change from oblate in the south to triaxial in the central part and magnetic foliation strikes east–west and dips to the north analog to tectonic foliation S1 (Fig. 7a site Z12). The magnetic lineation contained in the magnetic foliation and S1, trends NNE–SSW with moderate north–NE plunge ( $K_{\max}$  mean vector = 028/59,  $\alpha_{95} = 26.7^\circ$ ,  $k = 33.5$ ) (Fig. 7a site Z19). North-west of Yala Xiangbo and south of Yardoi three sites describe triaxial ellipsoids and magnetic foliation striking SW–NE with moderate dip values towards the NW. The cluster of  $K_{\max}$  values describes a magnetic lineation trending NNW–SSE with  $43^\circ$  plunge towards the north–NW (Fig. 8b). Moving towards Zetang and the Great Counter Thrust the AMS ellipsoid is oblate (sites Q16 and Q17) and magnetic foliation strikes NNW–ESE but with southward dip similar to S2 tectonic foliation (Figs 7a site Q16 & 8a). From these results we can define two domains within sector 2 with opposite dip of the magnetic foliation and tectonic foliation (Figs 7a & 8a).

Sector 3 lies geographically between north of the Dala pass and Qusum. Tectonically this area is east of the Cona Graben and south of the Qusum Thrust. Eastward of the Yala Xiangbo (sites Tu and We) AMS ellipsoids are triaxial, the magnetic foliation has a NW–SE strike and dips about  $60^\circ$  to the NE parallel to S1 (Fig. 7a site Tu2). The magnetic lineation trends NW–SE and plunges to the NW and SE. Moving to the north the magnetic foliation changes to east–west strike and the magnetic lineation becomes east–west with a gentle plunge to the east parallel to the intersection of S1 and S2 tectonic foliations. In the proximity of the Qusum Thrust and the S2 domain, the magnetic ellipsoid switches to be more prolate (e.g.  $T = -0.13$  in site Qu20). Here magnetic lineation trends east–west with almost horizontal plunge, parallel to the intersection of S1 and S2 tectonic foliations (Fig. 7b site Qu20 & Fig. 8b).

Sector 4 is located between the Great Counter Thrust and the Qusum Thrust where S2 is the main tectonic foliation. The southern and central parts present AMS ellipsoids which are slightly prolate (sites Mv27, Mv29, Fv38, Pa40) or oblate AMS ellipsoids (Fig. 7b site Mv27). The magnetic

foliation reflected in the oblate ellipsoids (sites Sr24, Sr25, Mv26, Mv28, Mv30 & Yt34) has WNW–ESE strike and south–SW dips parallel to S2 tectonic foliation. The slightly prolate ellipsoids present magnetic lineations with east–west direction and gentle plunges towards the west and are parallel to the F2 fold axes and the lineation defined by the intersection of S1 and S2 foliation. Towards the north, close to the Great Counter Thrust and the Indus Yarlung Suture Zone (sites Sr23, Yt32 & Yt33), ellipsoids turn to triaxial shape. Magnetic foliation trends west–east with steep dips towards the south and the magnetic lineation trends north–south with a  $67^\circ$  plunge to the south (sites Yt32 & Yt33), parallel to the stretching lineation and perpendicular to the Great Counter Thrust surface (Fig. 7b site Yt32 & Fig. 8a, b).

### Tectonic interpretation and sequence of magnetic fabric development

Magnetic foliation and lineation in the slates of the Triassic flysch are the result of a complex sum of tectonic and metamorphic phases from the India–Asia collision until present. We suggest a 5-stage-evolution of the magnetic fabric supported by the structural properties to constraint the kinematic evolution of the eastern Tethyan Himalaya. Magnetic foliation and lineation have been analysed referred to their present-day orientation (see Fig. 9 for kinematic model proposed here and Fig. 2 to comparison with other kinematic models previously proposed).

#### 1st Stage

During the Eohimalayan or D1 phase (Middle Eocene–Late Oligocene; Hodges 2000; Fig. 2) the collision of India and Asia produced the development of east–west-trending south facing isoclinal folds with related axial planar foliation (S1). This is shown south of Qonggyai (sector 2; Figs 4a & 8a) by well grouping  $K_{\min}$  directions and  $K_{\max}$  and  $K_{\text{int}}$  axes scattered within the tectonic S1 foliation plane (Fig. 9a).

#### 2nd Stage

Near the locality of Qonggyai where D1 phase governs the orientation of the structures, the magnetic lineation is interpreted as the direction of stretching lineation of the phyllosilicates, under the prevailing stress field, during thrust sheet emplacement as has been described in other thrust structures (Oliva-Urcia *et al.* 2009). The plunge of the magnetic lineation indicates thrust emplacement towards the south–SW (Himalayan foreland)

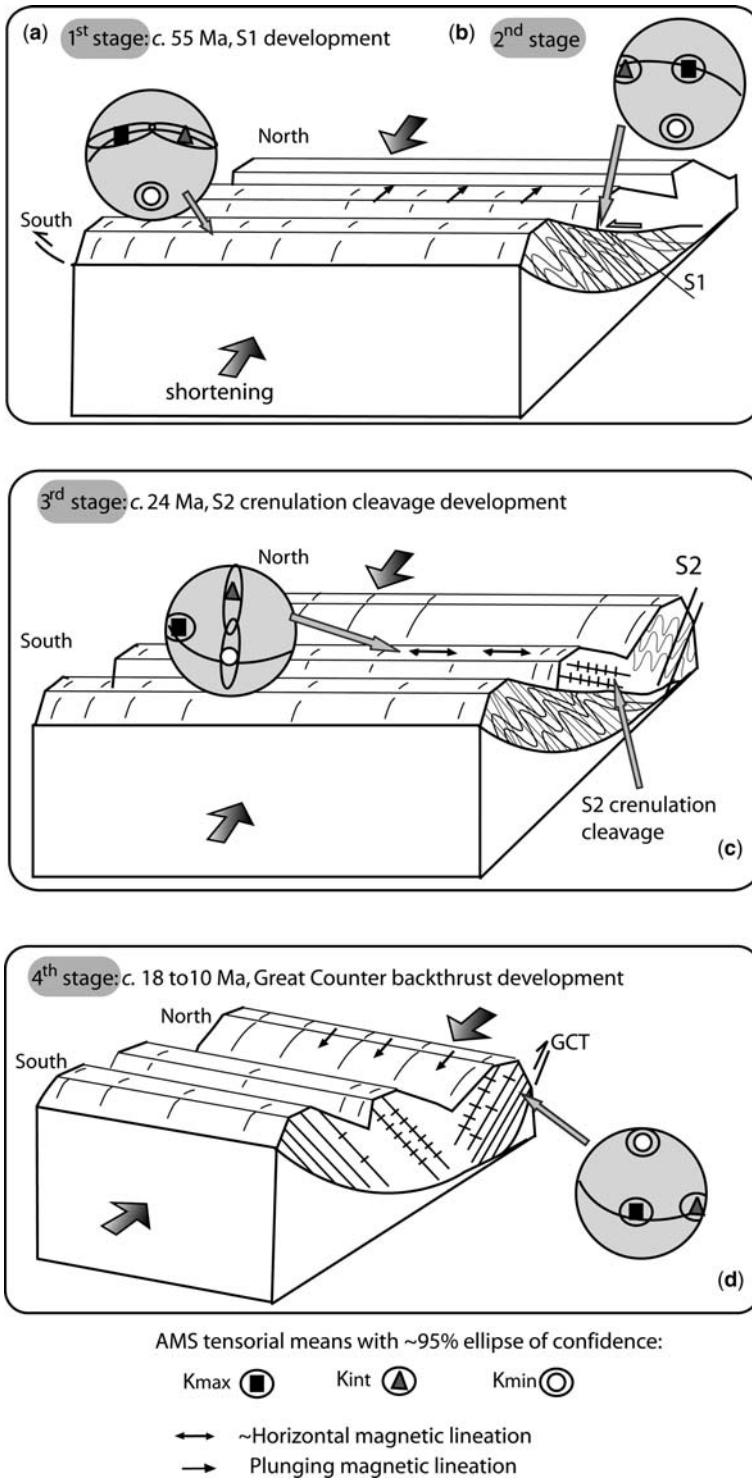


**Fig. 9.** Block diagrams showing the successive stages of the magnetic fabric evolution and the kinematics of the Triassic flysch in the eastern Tethyan Himalaya: (a) 1st stage, (b) 2nd stage, (c) 3rd stage and (d) 4th stage.

(Fig. 9b) in agreement with the south-directed displacement along the Lhunze fault, 15 km south of the studied sites (Aikman *et al.* 2008). Detailed structural and thermochronological analysis should be carried on the Lhunze Fault to closely constraint the timing and local and regional importance of this fault.

### 3rd Stage

Continuous deformation in the flysch thrust-wedge produced a change in the fold vergence around 20 km south of the Indus Yarlung Suture Zone and the Gangdese granite. This north-vergent deformation starts with the incipient development of the north-vergent F2 folds and related S2 crenulation cleavage (Fig. 2). This switch of vergence in the structures is recorded in the magnetic fabric by a subtle prolate ellipsoid with  $K_{\min}$  axes distributed in a semigirdle (Figs 7b sites Qu20, Mv27; Fig. 9c). This stage of magnetic fabric is similar to the stage of pencil cleavage (e.g. Borradaile & Tarling 1981; Housen *et al.* 1993; Parés *et al.* 1999) characterized by the incipient development of a new planar feature, in our case the foliation S2. This composite fabric reflects a combination of the S1 and the younger S2 foliation with  $K_{\max}$  axes strikingly east–west with gentle plunge, parallel to the intersection lineation between S1 and S2 (L12). The reason for this parallelism is that this direction is the intersection axis between the iron sheet silicates (Parés *et al.* 1999). As the foliation S2 becomes pervasive it transposes the older S1 and  $K_{\min}$  cluster parallel to the pole of S2 tectonic foliation.  $K_{\max}$  and  $K_{\text{int}}$  axes are distributed in a girdle that coincides with the S2 foliation plane. The time interval for the S2 foliation development can be related to the *c.* 24 Ma K/Ar ages found in illites (Dunkl *et al.* 2008), which we relate to an authigenic origin linked to the formation of the foliation S2. As deformation increases  $K_{\max}$  and  $K_{\min}$  axes become tightly clustered (triaxial ellipsoid) and magnetic lineation trends east–west parallel to F2 axes and the intersection lineation of S1 and S2 foliations (e.g. Fig. 8b sites Fv35 and Sr23).

### 4th Stage

Continuation of backward deformation towards higher structural levels was probably responsible for the formation of the north-directed Great Counter backthrust around 18 to 10 Ma (Quidelleur *et al.* 1997; Harrison *et al.* 2000; Fig. 2) which placed the Triassic flysch over the mélange complex or the Cretaceous rocks. This event is reflected in the north–south direction and 67° southward plunge of the magnetic lineation that is strikingly coincident with the stretching lineation in

sites Yt32 and Yt33. The magnetic lineation is the expression of the strain undergone by the hanging wall of the Great Counter backthrust during its emplacement (Fig. 9d).

### 5th Stage

From a more speculative point of view the 5th stage suggests two possible processes, which during the Middle Miocene resulted in the change of the east–west trend of the Eohimalayan magnetic foliation preserved in the Qonggyai valley to the NW–SE trend of the post-Eohimalayan magnetic foliation near Nagarze (sector 1) and east of the Cona Graben (sectors 3 and 4). The first possibility is an *c.* 20° clockwise rotation of the magnetic foliation related to vertical-axis rotations during the eastward extrusion of the Tibetan plateau (Tapponnier *et al.* 1982). Schill *et al.* (2004) also reported clockwise rotation in the central Tethyan Himalaya based on secondary remanence directions which were probably acquired during the last metamorphic cooling in Late Oligocene or Early Miocene times. Gan *et al.* (2007) describe a NE trend of GPS velocities in SE Tibet. Their data furthermore indicate that the GPS velocity east of the Cona Graben is more eastward directed which implies a clockwise rotation of this area relative to the adjacent area in the west. The second possibility can be associated with the doming of the North Himalayan domes. The magnetic foliation around the Yala Xiangbo describes a slight bend that is parallel to the contact of the dome with the flysch and in Nagarze area the inclination of the magnetic foliation and lineation decreases towards east of the flank of the Jangsang Lhamo dome. These two facts can suggest that the Triassic flysch had passively accommodated the doming around 18–13.5 Ma (Aikman *et al.* 2004) producing block rotations and tilting of the neighbouring structural elements.

## Conclusions

The AMS and structural data collected in the Triassic flysch of the Tethyan Himalaya indicate that the magnetic fabric is an indicator of progressive deformation when the original foliation is overprinted, and allow us to reconstruct the fabric and tectonic evolution processes in SE Tibet.

In the studied slates magnetic susceptibility is predominantly carried by the paramagnetic fraction. This is shown by temperature dependence of the susceptibility following the  $\sim 1/T$  Curie law, the comparison between the high field *v.* the low field susceptibilities and the parallelism between tectonic and magnetic foliation.

AMS provides quantitative information about the orientation of phyllosilicates alignment and the degree and shape of the AMS ellipsoid. Directions of stretching and intersection of the two foliations have been detected even when it is difficult to identify them in the field or only possible to measure them with extensive time consumption. AMS combined with structural studies allow us to gain a deeper structural insight on the evolution of the Triassic flysch within the eastern Tethyan Himalaya. Two different tectonic domains can be defined. East of the Cona graben these domains are separated by the Qusum Thrust. The southern domain is structurally dominated by east–west-striking and north-dipping magnetic foliation parallel to the Eohimalayan S1 tectonic foliation in accordance with the characteristic south vergence of the orogen. North of the Qusum Thrust ‘backward’ deformation is reflected in the magnetic foliation and tectonic S2 foliation which have WNW–ESE direction and dips to the south, opposite to the main vergence of the Himalayan system. In between the two domains an intermediate magnetic fabric is found where the incipient S2 foliation overlaps the S1 foliation and  $K_{\max}$  cluster roughly parallel to the intersection of S1 and S2 tectonic foliations. K/Ar age of *c.* 24 Ma (Dunkl *et al.* 2008) have been related to new micas with an authigenic origin linked to the formation of the S2 foliation. The two domains described in this study are the result of D1 and D2 deformation phases which can be observed in other north–south sections along the fold-thrust belt (Fig. 2), indicating no major changes in deformation features along east–west strike of the Tethyan Himalaya.

Magnetic lineation is interpreted as the transport direction of thrust structures in two locations within the study area. Near Qonggyai we identified a north–NE plunging magnetic lineation that is related to the phyllosilicates elongation direction, and could be the expression of the strain caused in the footwall of the Lhunze basement thrust. Close to the Yarlung Tsangpo, the magnetic lineation shows north–south trend and steep south plunge, and recorded the transport direction of the Neohimalayan Great Counter backthrust about 18 to 10 Ma (Quidelleur *et al.* 1997; Harrison *et al.* 2000) synchronous with the activity on the MCT and STDS (Yin *et al.* 1994).

Different orientations of magnetic foliations may indicate a Middle Miocene *c.* 20° clockwise vertical-axis rotation. This result would be in accordance with clockwise block rotations in the central Himalaya observed in secondary remanence directions (Schill *et al.* 2004) and present GPS velocities (e.g. Gan *et al.* 2007) that point out large-scale dextral shearing caused by the eastward extrusion of the Tibetan Plateau. Likewise intrusion and

exhumation of the North Himalayan domes can have induced block rotations and tilting of the adjacent tectonic elements. However these hypotheses need additional structural and palaeomagnetic analyses to be verified.

The authors thank the German Research Foundation (DFG) for financial support; Institute of Tibetan Plateau Research (ITP) and the Chinese Academy of Sciences (CAS) for logistic support. We thank Taba, Puchum, Nobu, and Xu Qiang for helping us during the field work. The authors are grateful to Zanist Hama-Aziz and Liu Yang for support in the magnetic measurements. We wish to thank B. Oliva-Urcia and R. Carosi for constructive comments. We deeply acknowledge the revisions from E. Pueyo, B. Housen, J. Poblet and R. Lisle which helped to improve the first version of the manuscript.

## References

- AIKMAN, A., HARRISON, T. M. & DING, L. 2004. Preliminary results from the Yala-Xiangbo Leucogranite dome, SE Tibet. *Himalaya Journal of Sciences*, **2**, 91.
- AIKMAN, A., HARRISON, T. M. & DING, L. 2008. Evidence for Early (>44 Ma) Himalayan Crustal Thickening, Tethyan Himalaya, southeastern Tibet. *Earth and Planetary Science Letters*, **274**, 14–23.
- APPEL, E., MÜLLER, R. & WIDDER, R. W. 1991. Palaeomagnetic results from the Tibetan Sedimentary Series of the Manang area (north central Nepal). *Geophysical Journal International*, **104**, 255–266.
- ARMJO, R., TAPPONNIER, P., MERCIER, J. L. & TONGLIN, H. 1986. Quaternary extension in southern Tibet: field observations and tectonic implications. *Journal of Geophysical Research*, **91**, 13 803–13 872.
- AVERBUCH, O., FRIZON DE LAMOTTE, D. & KISSEL, C. 1992. Magnetic fabric as a structural indicator of the deformation path within a fold-thrust structure: a test case from the Corbières (NE Pyrenees, France). *Journal of Structural Geology*, **14**, 461–474.
- BERTHÉ, D., CHOUKROUNE, P. & JEGOUZO, P. 1979. Orthogneiss, mylonite and non coaxial deformation of granites: the example of the South Armorican Shear Zone. *Journal of Structural Geology*, **1**, 31–42.
- BONHOMME, M. & GARZANTI, E. 1991. Age of metamorphism in the Zaskar Tethys Himalaya (India). *Géologie Alpine*, **16**, 15–16.
- BORRADAILE, G. J. & JACKSON, M. 2004. Anisotropy of magnetic susceptibility (AMS): magnetic petrofabric of deformed rocks. In: MARTÍN-FERNÁNDEZ, F., LÜNEBURG, C. M., AUBOURG, C. & JACKSON, M. (eds) *Magnetic Fabric: Methods and Applications*. Geological Society, London, Special Publications, **238**, 299–360.
- BORRADAILE, G. J. & SARVAS, P. 1990. Magnetic susceptibility fabrics in slates: structural, mineralogical and lithological influences. *Tectonophysics*, **172**, 215–222.
- BORRADAILE, G. J. & TARLING, D. H. 1981. The influence of deformation mechanism on magnetic fabrics in weakly deformed rocks. *Tectonophysics*, **77**, 151–168.
- BORRADAILE, G. J. & WERNER, T. 1994. Magnetic anisotropy of some phyllosilicates. *Tectonophysics*, **235**, 223–248.

- BOUCHEZ, J. L. 1997. Granite is never isotropic: an introduction to AMS studies of granitic rocks. *In*: BOUCHEZ, J. L., HUTTON, D. H. W. & STEPHEN, W. E. (eds) *Granite: From Segregation of Melt to Emplacement Fabrics*. Kluwer Academic Publishers, Dordrecht, 95–112.
- BROOKFIELD, M. 1993. The Himalayan passive margin from Precambrian to Cretaceous. *Sedimentary Geology*, **84**, 1–35.
- BURCHFIEL, B. C., ZHILIANG, C., HODGES, K. V., YUPING, L., ROYDEN, L. H., CHANGRONG, D. & JIENE, X. 1992. *The South Tibetan Detachment System, Himalaya Orogen: Extension Contemporaneous with and Parallel to Shortening in a Collisional Mountain Belt*. Geological Society of America, Special Papers, 269.
- BURG, J. P. & CHEN, G. M. 1984. Tectonics and structural zonation of southern Tibet, China. *Nature*, **311**, 219–223.
- BURMEISTER, K. C., HARRISON, M. J., MARSHAK, S., FERRÉ, E. C., BANNISTER, R. A. & KODAMA, K. P. 2009. Comparison of Fry strain ellipse and AMS ellipsoid trends to tectonic fabric trends in very low-strain sandstone of the Appalachian fold-thrust belt. *Journal of Structural Geology*, doi: 10.1016/j.jsg.2009.03.010.
- CAROSI, R., MONTOMOLI, C. & VISONÀ, D. 2002. Is there any detachment in the Lower Dolpo (western Nepal)? *Comptes Rendus Geoscience*, **334**, 933–940.
- CAROSI, R., MONTOMOLI, C. & VISONÀ, D. 2007. A structural transect in the Lower Dolpo: Insights on the tectonic evolution of Western Nepal. *Journal of Asian Earth Sciences*, **29**, 407–423, doi: 10.1016/j.jseas.2006.05.001.
- CHANG, C. 1984. Les caractéristiques tectoniques et l'évolution de la zone de suture du Yarlung-Zangbo. *In*: MERCIER, J. L. & LI, G. C. (eds) *Mission Franco-Chinoise Au Tibet 1980: Étude Géologique Et Géophysique De La Croûte Terrestre Et Du Manteau Supérieur Du Tibet Et De L'Himalaya*. Editions du Centre National de la Recherche Scientifique, Paris, France, 341–350.
- CHEN, Z., LIU, Y., HODGES, K. V., BURCHFIEL, B. C., ROYDEN, L. H. & DENG, C. 1990. The Kangmar dome: A metamorphic core complex in southern Xizang (Tibet). *Science*, **250**, 1552–1556.
- COLCHEN, M., LE FORT, P. & PÉCHER, A. 1986. *Annapurna-Manaslu-Ganesh Himal Notice De La Carte Géologique Au 1/200.000* (bilingual Edition, French–English). Centre National de la Recherche Scientifique, Paris.
- CROUZET, C., STANG, H., APPEL, E., SCHILL, E. & GAUTAM, P. 2001. Detailed analysis of successive pTRMs carried by pyrrhotite in Himalayan metacarbonates: an example from Hidden Valley Central Nepal. *Geophysical Journal International*, **146**, 607–618.
- CROUZET, C., DUNKL, I., PAUDEL, L., ARKAI, P., RAINER, T. M., BALOGH, K. & APPEL, E. 2007. Temperature and age constraints on the metamorphism of the Tethyan Himalaya in Central Nepal: a multidisciplinary approach. *Journal of Asian Earth Sciences*, **30**, 113–130, doi: 10.1016/j.jseas.2006.07.014.
- DING, L., KAPP, P. & WAN, X. 2005. Paleocene-Eocene record of ophiolite obduction and initial India–Asia collision, south central Tibet. *Tectonics*, **24**, TC3001, doi: 10.1029/2004TC001729.
- DUNKL, I., LIN, D. ET AL. 2008. Diagenetic and metamorphic overprint and deformation history of Permo-Triassic Tethyan sediments, SE Tibet. *Himalayan Journal of Sciences*, **5**, 49.
- DUPUIS, C., HÉBERT, R., DUBOIS-COTÉ, V., WANG, C. S., LI, Y. L. & LI, Z. J. 2005. Petrology and geochemistry of mafic rocks from mélange and flysch units adjacent to the Yarlung Zangbo Suture Zone, southern Tibet. *Chemical Geology*, **214**, 287–308.
- DUPUIS, C., HÉBERT, R., DUBOIS-COTÉ, V., GUILMETTE, C., WANG, C. S. & LI, Z. J. 2006. Geochemistry of sedimentary rocks from mélange and flysch units south of the Yarlung Zangbo suture zone, southern Tibet. *Journal of Asian Earth Sciences*, **26**, 489–508.
- EDWARDS, M. A. & HARRISON, T. M. 1997. When did the roof collapse? Late Miocene north–south extension in the high Himalaya revealed by Th–Pb monazite dating of the Khula Kangri granite. *Geology*, **25**, 543–546.
- FISHER, N. I., LEWIS, T. & EMBLETON, B. J. J. 1987. *Statistical Analysis of Spherical Data*. Cambridge University Press, Cambridge.
- FLINN, D. 1962. On folding during three-dimensional progressive deformation. *Quarterly Journal of the Geological Society of London*, **118**, 385–433.
- FUCHS, G. 1967. *Zum Bau Des Himalaya*. Osterreichische Akademie der Wissenschaften, Mathematisch-Naturwissenschaftliche Klasse, Denkschriften, **113**, 1–211.
- GAETANI, M. & GARZANTI, E. 1991. Multicyclic history of the northern Indian continental margin (northwestern Himalaya). *American Association of Petroleum Geologists, Bulletin*, **75**, 1427–1446.
- GAN, W., ZHANG, P. ET AL. 2007. Present-day crustal motion within the Tibetan Plateau inferred from GPS measurements. *Journal of Geophysical Research*, **112**, B08416, doi: 10.1029/2005JB004120.
- GANSSER, A. 1964. *Geology of the Himalayas*. Wiley Interscience, London.
- GARZANTI, E. 1999. Stratigraphy and sedimentary history of the Nepal Tethys Himalaya passive margin. *Journal of Asian Earth Sciences*, **17**, 805–827.
- GARZANTI, E., GORZA, M., MARTELLINI, L. & NICORA, A. 1994. Transition from diagenesis to metamorphism in the Paleozoic to Mesozoic succession of the Dolpo-Manang synclinorium and Thakkola graben (Nepal Tethys Himalaya). *Eclogae Geologicae Helveticae*, **87**, 613–632.
- GARZIONE, C. N., DECELLES, P. G., HODKINSON, D. G., OJHA, T. P. & UPRETI, B. N. 2003. East-west extension and Miocene environmental change in the southern Tibetan plateau: Thakkhola graben, central Nepal. *Geological Society of America Bulletin*, **115**, 3–20.
- GODIN, L. 2003. Structural evolution of the Tethyan sedimentary sequence in the Annapurna area, central Nepal Himalaya. *Journal of Asian Earth Sciences*, **22**, 307–328.
- GODIN, L., GRUJIC, D., LAW, R. D. & SEARLE, M. P. 2006. Channel flow, extrusion and exhumation in continental collision zones: an introduction. *In*: LAW, R. D., SEARLE, M. P. & GODIN, L. (eds) *Channel Flow, Ductile Extrusion and Exhumation in Continental*

- Collision Zones*. Geological Society, London, Special Publications, **268**, 1–23.
- GRUJIC, D., HOLLISTER, L. & PARRISH, R. R. 2002. Himalayan metamorphic sequence as an orogenic channel: insight from Bhutan. *Earth and Planetary Science Letters*, **198**, 177–191.
- GUILLOT, S., PÉCHER, A., ROCHETTE, P. & LEFORT, P. 1993. The emplacement of the Manaslu granite of central Nepal: field and magnetic susceptibility constraints. In: TRELOAR, P. J. & SEARLE, M. P. (eds) *Himalayan Tectonics*. Geological Society, London, Special Publications, **74**, 413–428.
- HARRISON, T. M., YIN, A., GROVE, M. & LOVERA, O. M. 2000. The Zedong Window: a record of superposed Tertiary convergence in southeastern Tibet. *Journal of Geophysical Research*, **105**, 19 211–19 320.
- HEIM, A. & GANSSER, A. 1939. Central Himalaya. Geological Observations of the Swiss Expedition 1936. *Mémoires de la Société Helvétique des Sciences Naturelles*, **7/31**, 1–245.
- HIRT, A. M., LOWRIE, W., CLENDENEN, W. S. & KLIGFIELD, R. 1988. The correlation of magnetic anisotropy with strain in the Chelmsford Formation of the Sudbury Basin, Ontario. *Tectonophysics*, **145**, 177–189.
- HODGES, K. V. 2000. Tectonics of the Himalaya and southern Tibet from two perspectives. *Geological Society of America Bulletin*, **112**, 324–350.
- HOLT, W. E., NI, J. F., WALLACE, T. C. & HAINES, A. J. 1991. The Active Tectonics of the Eastern Himalayan Syntaxis and Surrounding Regions. *Journal of Geophysical Research*, **96**, 14 595–14 632.
- HOUSEN, B. A., RICHTER, C. & VAN DER PLUIJM, B. A. 1993. Composite magnetic anisotropy fabrics: experiments, numerical models, and implications for the quantification of rock fabrics. *Tectonophysics*, **220**, 1–12.
- JELINEK, V. 1977. *The statistical theory of measuring anisotropy of magnetic susceptibility of rocks and its application*. Geofyzika Brno.
- KELLETT, D. A. & GODIN, L. 2009. Pre-Miocene deformation of the Himalayan superstructure, Hidden valley, central Nepal. *Journal of the Geological Society, London*, **166**, 261–275.
- KNEEN, S. 1976. The relationship between the magnetic and strain fabrics of some haematite-bearing Welsh slates. *Earth and Planetary Science Letters*, **31**, 413–416.
- LEE, J., HACKER, B. R. ET AL. 2000. Evolution of the Kangmar Dome, southern Tibet: structural, petrologic, and thermochronologic constraints. *Tectonics*, **19**, 872–895.
- LE FORT, P. 1975. Himalayas, the collided range. Present knowledge of the continental arc. *American Journal of Science*, **275-A**, 1–44.
- LIU, G. 1992. Permian to Eocene sediments and Indian passive margin evolution in the Tibetan Himalayas. *Tübinger Geowissenschaftliche*, **A13**, 1–268.
- LIU, G. & EINSELE, G. 1994. Sedimentary history of the Tethyan basin in the Tibetan Himalayas. *Geologische Rundschau*, **83**, 32–61.
- LIU, G. & EINSELE, G. 1996. Various types of olistostromes in a closing ocean basin, Tethyan Himalaya (Cretaceous, Tibet). *Sedimentary Geology*, **104**, 203–226.
- MARTÍN-HERNÁNDEZ, F. & HIRT, A. M. 2003. The anisotropy of magnetic susceptibility in biotite, muscovite and chlorite single crystals. *Tectonophysics*, **337**, 13–28.
- MCQUARRIE, N., ROBINSON, D., LONG, S., TOBGAY, T., GRUJIC, D., GEHRELS, G. & DUCEA, M. 2008. Preliminary stratigraphic and structural architecture of Bhutan: Implications for the along strike architecture of the Himalayan system. *Earth and Planetary Science Letters*, **272**, 105–117.
- MONTOMOLI, C., APPEL, E., ANTOLIN, B., DUNKL, I., EL BAY, R., LIN, D. & GLOAGUEN, R. 2008. Polyphase deformation history of the 'Tibetan Sedimentary Sequence' in the Himalaya chain (South-East Tibet). *Himalayan Journal of Sciences*, **5**, 91.
- NAGATA, T. 1961. *Rock Magnetism*. Maruzen, Tokyo.
- NAJMAN, Y., CARTER, A., OLIVER, G. & GARZANTI, E. 2005. Provenance of Eocene foreland basin sediments, Nepal: Constraints to the timing and diachroneity of early Himalayan orogenesis. *Geology*, **33**, 309–312.
- OLIVA-URCIA, B., LARRASOÑA, J. C. ET AL. 2009. Disentangling magnetic subfabrics and their link to deformation processes in cleaved sedimentary rocks from the Internal Sierras (west central Pyrenees, Spain). *Journal of Structural Geology*, **31**, 163–176.
- PAN, G., DING, J., YAO, D. & WANG, L. 2004. *Geological Map of Qinghai-Xizang (Tibet) Plateau and Adjacent Areas (1:1,500,000)*. Chengdu Institute of Geology and Mineral Resources, China Geological Survey. Chengdu Cartographic Publishing House.
- PARÉS, J. M. & VAN DER PLUIJM, B. 2002. Evaluating magnetic lineations (AMS) in deformed rocks. *Tectonophysics*, **350**, 283–298.
- PARÉS, J. M., VAN DER PLUIJM, B. A. & DINARÈS-TURELL, J. 1999. Evolution of magnetic fabric during incipient deformation of mudrocks (Pyrenees, northern Spain). *Tectonophysics*, **307**, 1–14.
- PATZELT, A., LI, H., WANG, J. & APPEL, E. 1996. Paleomagnetism of Cretaceous to Tertiary sediments from southern Tibet: evidence for the extent of the northern margin of India prior to the collision with Eurasia. *Tectonophysics*, **259**, 259–284.
- PÉCHER, A. 1991. The contact between the higher Himalayan crystalline sediments and the Tibetan sedimentary series: Miocene large-scale dextral shearing. *Tectonics*, **10**, 587–598.
- PUEYO, E. L., ROMÁN-BERDIEL, T., BOUCHEZ, J. L., CASAS, A. M. & LARRASOÑA, J. C. 2004. In: MARTÍN-FERNÁNDEZ, F., LÜNEBURG, C. M., AUBOURG, C. & JACKSON, M. (eds) *Magnetic Fabric: Methods and Applications*. Geological Society, London, Special Publications, **238**, 395–420.
- QUIDELLEUR, X., GROVE, M., LOVERA, O. M., HARRISON, T. M. & YIN, A. 1997. Thermal evolution and slip history of the Renbu-Zedong Thrust, southeastern Tibet. *Journal of Geophysical Research*, **102**, 2659–2679.
- RATSCHBACHER, L., FRISCH, W., LIU, G. & CHEN, C. 1994. Distributed deformation in southern and western Tibet during and after the India–Asia collision. *Journal of Geophysical Research*, **99**, 19 917–19 945.
- RICHTER, C. & VAN DER PLUIJM, B. A. 1994. Separation of paramagnetic and ferrimagnetic susceptibilities using low temperature magnetic susceptibilities and

- comparison with high field methods. *Physics of the Earth and Planetary Interiors*, **51**, 113–123.
- ROCHETTE, P. 1987. Metamorphic control of the magnetic mineralogy of black shales in the Swiss Alps: toward the use of 'magnetic isograds'. *Earth and Planetary Science Letters*, **84**, 1015–1020.
- ROMÁN-BERDIEL, T., CASAS, A. M., OLIVA-URCIA, B., PUEYO, E. & RILLO, C. 2004. The main Variscan deformation event in the Pyrenees: new data from the structural study of the Bielsa granite. *Journal of Structural Geology*, **17**, 1337–1346.
- SCHILL, E., APPEL, E., GODIN, L., CROUZET, C., GAUTAM, P. & REGMI, K. 2003. Record of deformation by secondary magnetic remanences and magnetic anisotropy in the Nar/Phu valley (central Himalaya). *Tectonophysics*, **377**, 197–209.
- SCHILL, E., APPEL, E., CROUZET, C., GAUTAM, P., WEHLAND, F. & STAIGER, M. 2004. Oroclinal bending v. regional significant clockwise rotations in the Himalayan arc—Constraints from secondary pyrrhotite remanences. In: SUSSMAN, A. J. & WEIL, A. B. (eds) *Orogenic Curvature: Integrating Paleomagnetic and Structural Analyses*. Geological Society of America, Special Paper, **383**, 73–85.
- SEARLE, M. 1986. Structural evolution and sequence of thrusting in the High Himalayan, Tibetan-Tethys and Indus suture zones of Zaskar and Ladakh, Western Himalaya. *Journal of Structural Geology*, **8**, 923–936.
- SOTO, R., MATTEI, M. & CASAS, A. M. 2003. Relationship between AMS and folding in an area of superimposed folding (Cotiella-Bóixols nappe, Southern Pyrenees). *Geodinamica Acta*, **16**, 171–185.
- STECK, A. 2003. Geological Map of the NW Himalaya. *Eclogae Geologicae Helvetiae*, **96**, 147–U13.
- STÖCKLIN, J. 1980. Geology of Nepal and its regional frame. *Journal of the Geological Society, London*, **137**, 1–34.
- TAPPONNIER, P., PELTZER, G., LE DAIN, A. Y., ARMIJO, R. & COBBOLD, P. 1982. Propagating extrusion tectonics in Asia: New insights from simple experiments with plasticine. *Geology*, **10**, 611–616.
- TARLING, D. H. & HROUDA, F. 1993. *The Magnetic Anisotropy of Rocks*. Chapman & Hall, London.
- VALDIYA, K. S. 1980. *Geology of the Kumaun Lesser Himalaya*. Wadia Institute of Himalayan Geology, Dehra Dun.
- WILLEMS, H., ZHOU, Z., ZHANG, B. & GRÄFE, K. U. 1996. Stratigraphy of the Upper Cretaceous and Lower Tertiary strata in the Tethyan Himalayas of Tibet (Tingri area, China). *Geologische Rundschau*, **85**, 723–754.
- YIN, A. 2006. Cenozoic evolution of the Himalayan Orogen as constrained by along strike variations of structural geometry, exhumation history, and foreland sedimentation. *Earth-Science Reviews*, **76**, 1–131.
- YIN, A. & HARRISON, T. M. 2000. Geologic evolution of the Himalayan–Tibetan orogen. *Annual Review of Earth and Planetary Sciences*, **28**, 211–280.
- YIN, A., HARRISON, T. M., RYERSON, F. J., WENJI, C., KIDD, W. & COPELAND, P. 1994. Tertiary structural evolution of the Gangdese thrust system, southeastern Tibet. *Journal of Geophysical Research*, **99**, 18 175–18 201.
- ZHANG, B., ZHANG, J., GUO, L. & WANG, W. 2005. Microstructural and deformational studies on mylonite in the detachment faults of Yalashangbo dome, North Himalayan domes zone. *Progress in Natural Science*, **15**, 1005–1013.